EUROPEAN ORGANISATION FOR PARTICLE PHYSICS

CERN–PPE/94–51
March 17, 1994

QCD Studies using a Cone-based Jet Finding Algorithm for e^+e^- Collisions at LEP

The OPAL Collaboration

Abstract

We describe a cone-based jet finding algorithm (similar to that used in $\overline{\mathrm{p}}\mathrm{p}$ experiments), which we have applied to hadronic events recorded using the OPAL detector at LEP. Comparisons are made between jets defined with the cone algorithm and jets found by the "JADE" and "Durham" jet finders usually used in e^+e^- experiments. Measured jet rates, as a function of the cone size and as a function of the minimum jet energy, have been compared with $\mathcal{O}(\alpha_s^2)$ QCD calculations, from which two complementary measurements of $\alpha_s(M_{Z^0})$ have been made. The results are $\alpha_s(M_{Z^0}) = 0.116 \pm 0.008$ and $\alpha_s(M_{Z^0}) = 0.119 \pm 0.008$ respectively, where the errors include both experimental and theoretical uncertainties. Measurements are presented of the energy flow inside jets defined using the cone algorithm, and compared with equivalent data from $\overline{\mathrm{p}}\mathrm{p}$ interactions, reported by the CDF collaboration. We find that the jets in e^+e^- are significantly narrower than those observed in $\overline{\mathrm{p}}\mathrm{p}$. The main contribution to this effect appears to arise from differences between quark- and gluon-induced jets.

(Submitted to Zeitschrift für Physik C)

The OPAL Collaboration

R. Akers[16], G. Alexander[23], J. Allison[16], K.J. Anderson[9], S. Arcelli[2], S. Asai[24], A. Astbury[28], D. Axen[29], G. Azuelos[18,a], A.H. Ball[17], R.J. Barlow[16], S. Barnett[16], R. Bartoldus[3], J.R. Batley[5], G. Beaudoin[18], A. Beck[23], G.A. Beck[13], J. Becker[10], C. Beeston[16], T. Behnke[27], K.W. Bell[20], G. Bella[23], P. Bentkowski[18], P. Berlich[10], S. Bethke[32], O. Biebel[3], I.J. Bloodworth[1], P. Bock[11], B. Boden[3], H.M. Bosch[11], M. Boutemeur[18], P. Bright-Thomas[25], R.M. Brown[20], A. Buijs[8], H.J. Burckhart[8], C. Burgard[27], P. Capiluppi[2], R.K. Carnegie[6], A.A. Carter[13], J.R. Carter[5], C.Y. Chang[17], C. Charlesworth[6], D.G. Charlton[8], S.L. Chu[4], P.E.L. Clarke[15], J.C. Clayton[1], I. Cohen[23], J.E. Conboy[15], M. Cooper[22], M. Coupland[14], M. Cuffiani[2], S. Dado[22], C. Dallapiccola[17], G.M. Dallavalle[2], C. Darling[31], S. De Jong[13], L.A. del Pozo[5], H. Deng[17], M. Dittmar[4], M.S. Dixit[7], E. do Couto e Silva[12], J.E. Duboscq[8], E. Duchovni[26], G. Duckeck[8], I.P. Duerdoth[16], D.J.P. Dumas[6], P.A. Elcombe[5], P.G. Estabrooks[6], E. Etzion[23], H.G. Evans[9], F. Fabbri[2], B. Fabbro[21], M. Fierro[2], M. Fincke-Keeler[28], H.M. Fischer[3], R. Folman[26], D.G. Fong[17], M. Foucher[17], H. Fukui[24], A. Fürtjes[8], A. Gaidot[21], J.W. Gary[4], J. Gascon[18], N.I. Geddes[20], C. Geich-Gimbel[3], S.W. Gensler[9], F.X. Gentit[21], T. Geralis[20], G. Giacomelli[2], P. Giacomelli[4], R. Giacomelli[2], V. Gibson[5], W.R. Gibson[13], J.D. Gillies[20], J. Goldberg[22], D.M. Gingrich[30,a], M.J. Goodrick[5], W. Gorn[4], C. Grandi[2], F.C. Grant[5], J. Hagemann[27], G.G. Hanson[12], M. Hansroul[8], C.K. Hargrove[7], P.F. Harrison[13], J. Hart[8], P.A. Hart[9], P.M. Hattersley[1], M. Hauschild[8], C.M. Hawkes[8], E. Heflin[4], R.J. Hemingway[6], G. Herten[10], R.D. Heuer[8], J.C. Hill[5], S.J. Hillier[8], T. Hilse[10], D.A. Hinshaw[18], P.R. Hobson[25], D. Hochman[26], R.J. Homer[1], A.K. Honma[28,a], R.E. Hughes-Jones[16], R. Humbert[10], P. Igo-Kemenes[11], H. Ihssen[11], D.C. Imrie[25], A. Jawahery[17], P.W. Jeffreys[20], H. Jeremie[18], M. Jimack[1], M. Jones[6], R.W.L. Jones[8], P. Jovanovic[1], C. Jui[4], D. Karlen[6], K. Kawagoe[24], T. Kawamoto[24], R.K. Keeler[28], R.G. Kellogg[17], B.W. Kennedy[15], J. King[13], S. Kluth[5], T. Kobayashi[24], M. Kobel[10], D.S. Koetke[8], T.P. Kokott[3], S. Komamiya[24], R. Kowalewski[8], R. Howard[29], J. von Krogh[11], J. Kroll[9], P. Kyberd[13], G.D. Lafferty[16], H. Lafoux[8], R. Lahmann[17], J. Lauber[8], J.G. Layter[4], P. Leblanc[18], P. Le Du[21], A.M. Lee[31], E. Lefebvre[18], M.H. Lehto[15], D. Lellouch[26], C. Leroy[18], J. Letts[4], L. Levinson[26], Z. Li[12], S.L. Lloyd[13], F.K. Loebinger[16], G.D. Long[17], B. Lorazo[18], M.J. Losty[7], X.C. Lou[8], J. Ludwig[10], A. Luig[10], M. Mannelli[8], S. Marcellini[2], C. Markus[3], A.J. Martin[13], J.P. Martin[18], T. Mashimo[24], P. Mättig[3], U. Maur[3], J. McKenna[29], T.J. McMahon[1], J.R. McNutt[25], F. Meijers[8], F.S. Merritt[9], H. Mes[7], A. Michelini[8], R.P. Middleton[20], G. Mikenberg[26], J. Mildenberger[6], D.J. Miller[15], R. Mir[12], W. Mohr[10], C. Moisan[18], A. Montanari[2], T. Mori[24], M. Morii[24], U. Müller[3], B. Nellen[3], H.H. Nguyen[9], S.W. O'Neale[1], F.G. Oakham[7], F. Odorici[2], H.O. Ogren[12], C.J. Oram[28,a], M.J. Oreglia[9], S. Orito[24], J.P. Pansart[21], P. Paschievici[26], G.N. Patrick[20], M.J. Pearce[1], P. Pfister[10], J.E. Pilcher[9], J. Pinfold[30], D. Pitman[28], D.E. Plane[8], P. Poffenberger[28], B. Poli[2], T.W. Pritchard[13], H. Przysiezniak[18], G. Quast[27], M.W. Redmond[8], D.L. Rees[8], G.E. Richards[16], M. Rison[5], S.A. Robins[13], D. Robinson[5], A. Rollnik[3], J.M. Roney[28], E. Ros[8], S. Rossberg[10], A.M. Rossi[2], M. Rosvick[28], P. Routenburg[30], K. Runge[10], O. Runolfsson[8], D.R. Rust[12], M. Sasaki[24], C. Sbarra[2], A.D. Schaile[26], O. Schaile[10], F. Scharf[3], P. Scharff-Hansen[8], P. Schenk[4], B. Schmitt[3], H. von der Schmitt[11], M. Schröder[12], H.C. Schultz-Coulon[10], P. Schütz[3], M. Schulz[8], C. Schwick[27], J. Schwiening[3], W.G. Scott[20], M. Settles[12], T.G. Shears[5], B.C. Shen[4], C.H. Shepherd-Themistocleous[7], P. Sherwood[15], G.P. Siroli[2], A. Skillman[16], A. Skuja[17], A.M. Smith[8], T.J. Smith[28], G.A. Snow[17], R. Sobie[28], R.W. Springer[17], M. Sproston[20], A. Stahl[3], C. Stegmann[10], K. Stephens[16], J. Steuerer[28], R. Ströhmer[11], D. Strom[19], H. Takeda[24], S. Tarem[8], M. Tecchio[9], P. Teixeira-Dias[11], N. Tesch[3],

M.A. Thomson[15], E. Torrente-Lujan[22], S. Towers[6], N.J. Tresilian[16], T. Tsukamoto[24], M.F. Turner[8], D. Van den plas[18], R. Van Kooten[12], G.J. VanDalen[4], G. Vasseur[21], M. Vincter[28], A. Wagner[27], D.L. Wagner[9], C. Wahl[10], C.P. Ward[5], D.R. Ward[5], J.J. Ward[15], P.M. Watkins[1], A.T. Watson[1], N.K. Watson[7], P. Weber[6], P.S. Wells[8], N. Wermes[3], B. Wilkens[10], G.W. Wilson[4], J.A. Wilson[1], V-H. Winterer[10], T. Wlodek[26], G. Wolf[26], S. Wotton[11], T.R. Wyatt[16], R. Yaari[26], A. Yeaman[13], G. Yekutieli[26], M. Yurko[18], W. Zeuner[8], G.T. Zorn[17].

[1]School of Physics and Space Research, University of Birmingham, Birmingham B15 2TT, UK
[2]Dipartimento di Fisica dell' Università di Bologna and INFN, I-40126 Bologna, Italy
[3]Physikalisches Institut, Universität Bonn, D-53115 Bonn, Germany
[4]Department of Physics, University of California, Riverside CA 92521, USA
[5]Cavendish Laboratory, Cambridge CB3 0HE, UK
[6]Carleton University, Department of Physics, Colonel By Drive, Ottawa, Ontario K1S 5B6, Canada
[7]Centre for Research in Particle Physics, Carleton University, Ottawa, Ontario K1S 5B6, Canada
[8]CERN, European Organisation for Particle Physics, CH-1211 Geneva 23, Switzerland
[9]Enrico Fermi Institute and Department of Physics, University of Chicago, Chicago IL 60637, USA
[10]Fakultät für Physik, Albert Ludwigs Universität, D-79104 Freiburg, Germany
[11]Physikalisches Institut, Universität Heidelberg, D-69120 Heidelberg, Germany
[12]Indiana University, Department of Physics, Swain Hall West 117, Bloomington IN 47405, USA
[13]Queen Mary and Westfield College, University of London, London E1 4NS, UK
[14]Birkbeck College, London WC1E 7HV, UK
[15]University College London, London WC1E 6BT, UK
[16]Department of Physics, Schuster Laboratory, The University, Manchester M13 9PL, UK
[17]Department of Physics, University of Maryland, College Park, MD 20742, USA
[18]Laboratoire de Physique Nucléaire, Université de Montréal, Montréal, Quebec H3C 3J7, Canada
[19]University of Oregon, Department of Physics, Eugene OR 97403, USA
[20]Rutherford Appleton Laboratory, Chilton, Didcot, Oxfordshire OX11 0QX, UK
[21]DAPNIA/SPP, Saclay, F-91191 Gif-sur-Yvette, France
[22]Department of Physics, Technion-Israel Institute of Technology, Haifa 32000, Israel
[23]Department of Physics and Astronomy, Tel Aviv University, Tel Aviv 69978, Israel
[24]International Centre for Elementary Particle Physics and Department of Physics, University of Tokyo, Tokyo 113, and Kobe University, Kobe 657, Japan
[25]Brunel University, Uxbridge, Middlesex UB8 3PH, UK
[26]Particle Physics Department, Weizmann Institute of Science, Rehovot 76100, Israel
[27]Universität Hamburg/DESY, II Institut für Experimental Physik, Notkestrasse 85, D-22607 Hamburg, Germany
[28]University of Victoria, Department of Physics, P O Box 3055, Victoria BC V8W 3P6, Canada
[29]University of British Columbia, Department of Physics, Vancouver BC V6T 1Z1, Canada
[30]University of Alberta, Department of Physics, Edmonton AB T6G 2J1, Canada
[31]Duke University, Dept of Physics, Durham, NC 27708-0305, USA
[32]Universität Aachen, III Physikalisches Institut, Sommerfeldstrasse 26-28, D-52056 Aachen, Germany

[a]Also at TRIUMF, Vancouver, Canada V6T 2A3

1 Introduction

Many analyses of the hadronic final states produced in e^+e^- collisions rely upon algorithms which group the observed hadrons into jets. In studies of QCD the jets may be used to infer the dynamics of underlying quarks and gluons described by perturbative calculations. For example, measurements of jet rates provide one of the most intuitive approaches to the determination of α_s, while angular correlations between jets can be used to test details of the QCD matrix elements. Jet finding is also commonly used in studies of the b-quark. For example, possible tagging techniques involve the observation of a lepton emitted at high transverse momentum with respect to the parent hadron, or the reconstruction of a secondary vertex from the decay products of a b-flavoured hadron. The momentum vector of a jet will typically be used to estimate the direction of the b-quark or of a b-flavoured hadron, or a jet may be used to define the particles amongst which secondary vertices are sought.

The algorithms commonly used for jet finding in e^+e^- interactions are substantially different from those generally used in $\overline{p}p$ experiments. In e^+e^- studies, the "JADE" algorithm [1], and variants thereof, are most often used. In the original form of the JADE scheme, referred to as "E0", a scaled invariant mass y_{ij} is formed between all pairs of particles or jets. Pairs of four-momenta are combined into jets, starting with the smallest y_{ij}, until all y_{ij} values exceed some cutoff y_{cut}, which determines the jet resolution. The recently invented "Durham" scheme [2, 3] is similar, but with y_{ij} redefined as a scaled relative transverse momentum between a pair of particles; this scheme has the advantage that it can be treated by resummed QCD calculations [4]. Some comparisons between these jet finding schemes, and variants of them, may be found in Ref. [2].

In $\overline{p}p$ experiments, in contrast, jet finders have generally been based on defining as a jet a group of particles whose momentum vectors lie within a cone (see e.g. Ref. [5, 6]). Such a definition of a jet is intuitively reasonable at high energies, where jets are seen as highly collimated groups of hadrons, and was indeed suggested long ago in the context of e^+e^- hadronic events [7]. Cone-based algorithms have tended to be preferred in hadron collisions, where calorimetric measurements of energy flow are typically used, and where part of the energy of the event (the spectator jets) is in the form of particles of low transverse momentum, many of which may lie close to the beam directions, and therefore be undetected. Some standardization of the algorithm used for jet finding in hadron-hadron experiments was attempted in the "Snowmass proposal" [8]. However, the use of different jet finding algorithms in e^+e^- and $\overline{p}p$ experiments makes it difficult to compare the properties of jets produced in the two environments. An algorithm based on an angular definition of jets was used in some of the early e^+e^- jet studies at PETRA [9], but was not really comparable with the $\overline{p}p$ jet finders.

In the present study we have therefore implemented a cone-based jet finding algorithm, and applied it to e^+e^- data from the OPAL detector at LEP. A brief account of the OPAL detector and data analysis procedures is given in Sect. 2. In Sect. 3 we describe the algorithm in detail. In Sect. 4 we compare the performance of the cone jet finder with the conventional JADE-type schemes. In Sect. 5 we compare jet rates measured using the cone algorithm with $\mathcal{O}(\alpha_s^2)$ QCD calculations; this allows us to make new determinations of the strong coupling constant $\alpha_s(M_{Z^0})$. In Sect. 6 we compare jets in e^+e^- collisions with recent $\overline{p}p$ data, by measuring the energy flow within cone jets. Finally in Sect. 7 we summarize our findings, and make some

suggestions about the possible uses and benefits of the cone algorithm.

2 The OPAL Detector and Data Selection

A detailed description of the OPAL detector has been presented in Ref. [10], and therefore only a brief account of the main features relevant to the present analysis will be given here.

The momenta of charged particles are measured in the central tracking detectors, specifically in three drift chamber systems. The central detectors lie within an axial magnetic field of 0.435 T. A precision vertex chamber, of radius 24 cm and a length of 100 cm, provides space points with a resolution of about 50 μm in the r-ϕ plane*. Surrounding this is a large jet chamber, of radius 185 cm and length about 400 cm, which provides up to 159 digitizations per track with an r-ϕ resolution of around 130 μm. On the outside lies a system of thin chambers, with a resolution of about 300 μm in z, to improve the determination of θ.

The electromagnetic calorimeter consists of a barrel of 9440 lead glass blocks oriented so that they nearly point to the interaction region, and two endcaps of 1132 lead glass blocks each, aligned along the z-axis. The overall coverage is about 98% of 4π. In addition to measuring the energies of electrons and photons, the electromagnetic calorimeter records a substantial fraction of the energy of charged and neutral hadrons.

The OPAL trigger [12] contains a high degree of redundancy, so that the efficiency for accepting multihadronic events is greater than 99.9%. The online and offline selection procedures are described in Refs. [13, 14], and are also highly efficient. For the present analysis further cuts were applied to remove residual background and provide a sample of well contained events. The centre-of-mass energy was required to lie within 0.5 GeV of the Z^0 mass. Charged tracks were accepted for this analysis if they satisfied the following criteria: transverse momentum with respect to the beam axis greater than 0.15 GeV/c, at least 40 reconstructed points in the jet chamber, extrapolation to the collision point within 2 cm in r-ϕ and 25 cm in z and measured momentum less than 60 GeV/c. The number of such tracks was required to be at least five to reduce $\tau^+\tau^-$ background. Clusters of electromagnetic energy were used if their observed energy was greater than 0.25 GeV, and known noisy channels in the detector were removed. In order to ensure containment of the events the thrust axis [15] was determined using all tracks and clusters satisfying the above criteria, and was required to satisfy $|\cos\theta| < 0.9$. Monte Carlo studies indicate that, with these selection criteria, 99.86$\pm$0.07% of hadronic Z^0 decays are accepted within the chosen range of $\cos\theta$, with a contamination of about 0.14% from $\tau^+\tau^-$ events, and around 0.07% from two-photon interactions. Using the OPAL data collected in 1991 a data sample of 240,621 events remained after these cuts.

*The OPAL coordinate system is defined so that z is the coordinate parallel to the e^- beam, r is the coordinate normal to this axis, θ is the polar angle with respect to z and ϕ is the azimuthal angle about the z-axis.

3 The Cone Jet Finding Algorithm

The algorithm described here is intended to correspond closely to the Snowmass proposal [8], and to the algorithm used by the CDF experiment [6]. A jet is defined as a set of particles whose momentum vectors lie within a cone of half-angle R, such that the axis of the cone coincides with the momentum sum of the particles contained[†]. The total energy of the set of particles is required to be greater than some cutoff ε. Thus the results of the jet finding depend on two parameters, R and ε. Typical values would be 0.7 rad and 7 GeV respectively, which, as discussed below, are found to give good performance for the jet finder. It is possible for the cones of two such jets to overlap in space, and therefore for particles to be assigned to more than one jet. The special treatment needed in these cases is described below.

- Each particle in the event is considered in turn, and its momentum vector is taken as the axis of a cone of half angle R. All particles lying within this cone are found and their momenta summed. If the momentum sum and the cone axis do not coincide, the momentum sum is taken to define a new cone axis and the process is iterated. When a stable solution has been reached, the particles in the cone are deemed to constitute a "proto-jet". Unless the set of particles forming the proto-jet is identical to one already found, the new proto-jet is added to a list. When the algorithm is applied to OPAL data with R=0.7 rad, five proto-jets per event are found on average at this stage. The cone size R=0.7 rad is the value recommended in Ref. [8], and also proves to give good performance for the e^+e^- case, as discussed below.

- If two narrow jets are separated by an angle between R and $2R$, they could be found as two separate proto-jets at this stage. To permit this configuration to be found as a single jet, for each pair of proto-jets the direction which bisects the angle between their axes is also considered as a possible initial cone axis, and an iterative search for further stable proto-jets is performed. If a new proto-jet is found, it will generally overlap with the other proto-jets, which will be eliminated at a later stage.

- Proto-jets with energy less than ε are rejected. After this cut, with R=0.7 rad and ε=7 GeV, 2.6 proto-jets per event survive on average.

- Cases are identified where the cones of proto-jets overlap. The objective is to ensure that no particle is assigned to more than one jet. There are four possible cases:

  - If the cones of two proto-jets overlap, but no particles are contained in the overlapping region, no action is taken.
  - If the particles comprising one proto-jet are all contained in another proto-jet, the first proto-jet is eliminated.
  - Otherwise, if two proto-jets have some particles in common, the overlap fraction f is computed as the ratio of the total energy of the particles common to both proto-jets to the energy of the lower energy proto-jet. If $f > 0.75$ the particles in common are

[†]It is possible to apply the algorithm to the tracks and clusters of electromagnetic energy observed in the OPAL detector, or to the partons generated in a QCD Monte Carlo program or to the hadrons formed from them. Whichever is chosen, they are referred to as "particles" in the description of the algorithm.

assigned to the higher energy proto-jet, and the lower energy proto-jet is eliminated. If multiple overlaps occur, the highest energy pairs are treated first.

- If $f < 0.75$ each particle in the overlap region is assigned to the proto-jet to which it lies closest in angle. Most overlaps tend to have f close to zero or one, so the results are rather insensitive to the precise choice of the cut on f; we have chosen to use the same value as the CDF collaboration [6].

If particles have been reassigned in this treatment of overlaps, the jet momentum is recomputed as the sum of the momenta of the particles contained in the jet, and may no longer exactly coincide with the axis of the original cone.

- Proto-jets with energy less than ε are again rejected and the remainder form the final set of jets. With R=0.7 rad and ε=7 GeV, 2.3 jets per event are found on average in OPAL data.

There are still some small differences between the present algorithm and the algorithms used in $\overline{\mathrm{p}}\mathrm{p}$ experiments. These differences stem from the fact that in hadron collisions the centre-of-mass of the hard collision is in general boosted in the laboratory frame. The effect of these residual differences prove to be small, as discussed in Sect. 6.2 below. In discussion later we shall refer to our standard algorithm as operating in the "E-χ" metric, χ being the angle between a particle and the jet axis.

4 Comparison with other Jet Finders

The cone jet finder differs in many respects from the conventional JADE-type algorithms, which leads to several significant differences between the resulting jets when the two algorithms are used. In the JADE jet finders, every particle is assigned to a jet, while in the cone scheme there may be soft particles which lie far away from all the cone axes and are not assigned to any jet. Using R=0.7 rad and ε=7 GeV there are on average 6 unassigned particles per event, amounting to about 4% of the visible energy E_{vis}. In the JADE-type schemes, some of the particles associated to a jet may lie at a large angle to the jet direction, up to 180°, while in the cone jet finder all the particles in a jet lie close in angle to the jet axis. With the JADE-type algorithms, the number of jets falls monotonically as the resolution parameter y_{cut} is increased, and when an event changes from three-jet to two-jet (say), two jets merge into one. In the cone scheme, the number of jets (usually, but not always [16]) falls as ε is increased, but when an event changes from three-jet to two-jet one of the jets is simply eliminated, and the others remain essentially unchanged. The situation when R is varied is more complicated; as R is increased two jets may become merged into one, reducing the number of jets, or more particles may be included in a proto-jet, so moving it above the threshold ε and increasing the number of jets.

In order to make quantitative comparisons between the jet finding algorithms we have examined Monte Carlo events, generated using the JETSET parton shower model [17], and processed through the OPAL detector simulation program [18]. It is desirable that the jets reconstructed in the OPAL detector should reflect the structure of the events at the parton

level. Accordingly, the jet finding algorithms were run on the partons generated at the end of the parton shower, on the stable hadrons (those with lifetimes greater than 3×10^{-10} s) at the end of the hadronization process, and on the detected tracks and clusters of electromagnetic energy. In order to make comparisons, the jets were matched between pairs of levels (parton and hadron or hadron and detector) by finding the permutations which minimized the sum of the angles between pairs of jets at the two levels. When the numbers of jets at two levels were not equal, the best match of the smaller number of jets was found.

We define the following quantities to characterize the quality of the jet. Each is defined by comparing the jets at two levels, A and B. If A is the parton level and B the hadron level the comparison gives information about hadronization effects, while if A is the hadron level, and B is the detector level we obtain a measure of the effects of detector acceptance and resolution.

The jet energy resolution, σ_E, is the r.m.s. deviation of the distribution of the difference in energy between the jets found at level A and the corresponding jets found at level B, and therefore represents the average energy resolution per jet. We calculate σ_E separately for cases where two, three and four jets are matched. In the case of jets at the detector level, all energies are divided by a factor E_{vis}/E_{cm} to account for undetected energy, where E_{cm} is the centre-of-mass energy, and E_{vis} the total energy of all tracks and energy clusters used in the analysis.

The jet angular resolution, σ_θ, is the mean of the distribution of the sum of the angles between the jets found at level A and the corresponding jets found at level B. We calculate σ_θ separately for cases where two, three and four jets are matched. Since σ_θ involves a sum over the jets, it may be expected to increase with the number of jets.

The jet number efficiency, ζ_n, is the fraction of n-jet events at level A which are found to contain exactly n jets at level B.

The jet number purity, ρ_n, is the fraction of n-jet events found at level B which were found to be n-jet events at level A.

We find that the largest values of ζ and ρ are obtained for values of the jet finder parameters R and ε around 0.7 rad and 7 GeV respectively, which we therefore regard as the canonical values throughout this paper. With these values, most events are classified as two-jet, with about 20-25% of three-jet events, and typically 3% of four-jet events. As ε is varied at fixed R, we find that both σ_E and σ_θ tend to become smaller as ε is increased, especially for three- and four-jet events. As R is varied at fixed ε we observe that σ_E falls with increasing R as a result of hadronization effects, while σ_θ increases with increasing R because of detector effects.

In order to compare the cone jet finder with the JADE-type schemes, we take the cone algorithm with R=0.7 rad and ε=7 GeV, the JADE-E0 jet finder with y_{cut}=0.06, the JADE-p jet finder [2] with y_{cut}=0.05 and the Durham scheme with y_{cut}=0.02. With these parameters, the four jet finders yield roughly equal rates for two-, three- and four-jet production. In Figure 1 we show the resolutions, efficiencies and purities associated with hadronization effects for the four schemes, and in Figure 2 we show the corresponding results for detector effects. The same sample of about 25,000 Monte Carlo events was used for each algorithm. In broad terms the performance of the four jet finders is comparable. The cone algorithm is found to give improved

angular resolution, σ_θ, particularly when detector effects are considered, and somewhat better energy resolution, σ_E, with regard to hadronization effects, though not as good as the JADE-p scheme. However, the jet number efficiency and purity with regard to hadronization tend to be lower for the cone algorithm, indicating that hadronization corrections to the jet multiplicities will be greater for cone jets.

5 Jet Production Rates, and Comparison with $\mathcal{O}(\alpha_s^2)$ QCD Predictions

We have compared the jet rates measured with the cone jet finder with the predictions of $\mathcal{O}(\alpha_s^2)$ QCD. This has been done in two ways; we measure the jet rates as a function of ε at fixed R=0.7 rad, and as a function of R at fixed ε=7 GeV. As a result of these comparisons we are able to make two completely new measurements of $\alpha_s(M_{Z^0})$. In contrast to the traditional JADE-type schemes, the cone jet finder allows us to make two complementary tests of QCD using the same algorithm, so that we can check whether QCD can account for the dependence of jet rates on both R and ε with a common value of $\alpha_s(M_{Z^0})$. Roughly speaking, the dependence on R is sensitive to the angular distribution of gluon emission, while the dependence on ε is sensitive to the momentum distribution; in the JADE-type schemes invariant masses or transverse momenta are formed which use a combination of angular and momentum information.

The experimental procedure adopted followed closely that described in a recent OPAL paper [19]. For each event the number of jets was calculated using the observed tracks and clusters for several values of ε fixing R=0.7 rad and for several values of R at ε=7 GeV; from this the average two-, three- and four-jet rates (R_2, R_3 and R_4, where $R_n = \sigma_{n-jet}/\sigma_{tot}$) were computed. These jet rates were then corrected for detector effects (and, before comparing with the QCD theory, for hadronization effects also) using the bin-by-bin correction procedure described in Refs. [20, 19]. In Fig. 3 we show the measured jet rates R_2, R_3 and R_4 at the hadron level (i.e. corrected for detector effects only) as a function of ε and of R. The measured jet rates are also given in Table 1. For comparison, the predictions of the parton shower models JETSET[‡] [17], HERWIG[§] [21] and ARIADNE[¶] [23] are also shown in Fig. 3. The agreement is generally good. We also show in Fig. 3 the percentage differences between the models and the data, defined as $\delta_n = 100 \cdot (R_n^{model} - R_n^{data})/R_n^{data}$.

The measured jet rates such as R_2 are strongly correlated between neighbouring bins, because an event which has two jets at some value of ε (say) is likely to remain a two-jet event at nearby values of ε. By analogy with the previous OPAL analyses of jet rates [24, 25, 26] we have therefore defined the differential two-jet rates:

$$D_2(\varepsilon) = \frac{R_2(\varepsilon + \frac{1}{2}\Delta\varepsilon) - R_2(\varepsilon - \frac{1}{2}\Delta\varepsilon)}{\Delta\varepsilon}$$

[‡] The standard OPAL parameters for JETSET version 7.3 were determined in Ref. [20] from a fit to OPAL global event shape data.

[§] The standard OPAL parameters for HERWIG version 5.5 are given in Ref. [22]

[¶] The standard OPAL parameters for ARIADNE version 3.1 were determined in Ref. [20].

where R was fixed to 0.7 rad, and

$$D_2(R) = \frac{R_2(R + \frac{1}{2}\Delta R) - R_2(R - \frac{1}{2}\Delta R)}{\Delta R}$$

in which ε was fixed to 7 GeV. The bin widths $\Delta\varepsilon$ and ΔR are given by the differences between adjacent values of ε or R in Table 1. In the case of the JADE-type jet finders each event would just enter once in the corresponding $D_2(y_{cut})$ distribution, at the value of y_{cut} at which the event changed from two- to three-jet, and therefore the measured data points would be uncorrelated. This is not quite the case for the cone jet finder, because the number of jets does not always vary monotonically with ε or R. However, these complications affect only a small fraction of events, so in fitting the data we have neglected any residual correlations.

To $\mathcal{O}(\alpha_s^2)$ the strong coupling constant may be written (following the convention of Ref. [27]):

$$\alpha_s(\mu) = \frac{1}{\beta_0 \ln(\mu^2/\Lambda^2_{\overline{MS}})}\left[1 - \frac{\beta_1 \ln(\ln(\mu^2/\Lambda^2_{\overline{MS}}))}{\beta_0^2 \ln(\mu^2/\Lambda^2_{\overline{MS}})}\right] \quad , \tag{1}$$

where $\beta_0 = (33 - 2n_f)/12\pi$, $\beta_1 = (153 - 19n_f)/24\pi^2$ and n_f is the number of quark flavours, taken to be five. The QCD scale $\Lambda_{\overline{MS}}$ refers to the $\overline{MS}$ renormalization scheme [28]. The $\mathcal{O}(\alpha_s^2)$ QCD predictions for $D_2(\varepsilon)$ and $D_2(R)$ can be written in the form [29] (writing y for ε or R):

$$D_2(y) = A(y)\overline{\alpha}_s(\mu) + [B(y) + 2\pi\beta_0 \ln(x_\mu^2)A(y)]\overline{\alpha}_s^2(\mu)$$

where the renormalization scale μ is related to the centre of mass energy E_{cm} by $\mu = x_\mu E_{cm}$, and $\overline{\alpha}_s = (\alpha_s/2\pi)$. The significance of the renormalization scale factor, x_μ, will be considered below. The coefficients $A(y)$ and $B(y)$ were computed by integrating the $\mathcal{O}(\alpha_s^2)$ matrix elements [30] using the program EVENT as used by the authors of Ref. [29]. These QCD predictions have been fitted to the measured data (corrected to the parton level) using a least χ^2 method to determine the value of $\Lambda_{\overline{MS}}$, and thus of $\alpha_s(M_{Z^0})$ using eqn.(1). The fits were carried out in the ranges $7 < \varepsilon < 21$ GeV for $D_2(\varepsilon)$ and 0.3 rad$< R <$1.3 rad for $D_2(R)$, these representing the largest regions over which a satisfactory fit could be obtained (with both $\Lambda_{\overline{MS}}$ and x_μ fitted). For each distribution two fits were carried out: one in which x_μ was fixed to unity, and one in which x_μ was treated as a free parameter to be determined by the fit. It is generally understood that allowing x_μ to be optimized in the fit accounts, in a crude way, for some of the missing higher order terms in the theory [24]. There is therefore no reason to expect the optimal values of x_μ for $D_2(\varepsilon)$ and $D_2(R)$ to be equal, since they are likely to be subject to different higher order effects. The fit results are given in Table 2, and the fitted functions are compared with the data in Fig. 4.

We note that the fits to the data with x_μ=1 are poor. However, by allowing the renormalization scale factor x_μ to vary, an acceptable description of the data by $\mathcal{O}(\alpha_s^2)$ QCD may be obtained in both cases. The value of χ^2/d.o.f. for $D_2(\varepsilon)$ is, however, significantly greater than unity; this may be because (following our previous procedure [19, 24]) systematic uncertainties in the measurements have not been taken into account when calculating χ^2, or because of the effect of missing higher order terms which are only partially accounted for by the scale optimization. In Fig. 5 we show the variation of χ^2/d.o.f. and $\alpha_s(M_{Z^0})$ with x_μ. As for the JADE-type jet schemes, and for most other observables analysed in $\mathcal{O}(\alpha_s^2)$ [24], the data show a marked preference for small values of x_μ. The value of $\alpha_s(M_{Z^0})$ obtained from $D_2(\varepsilon)$ shows significant dependence on x_μ, taking a minimum close to the minimum in χ^2/d.o.f.; this behaviour is again

reminiscent of the JADE-type schemes. In contrast, the value of $\alpha_s(M_{Z^0})$ obtained from $D_2(R)$ exhibits very little dependence on x_μ, even though the χ^2/d.o.f. behaviour shows a pronounced minimum.

Systematic errors on the measurements of $\alpha_s(M_{Z^0})$ have been assigned following the procedures of Refs. [19, 24]. The individual contributions are tabulated in Table 3, from which their degree of correlation may be judged, together with the statistical errors. They may be summarized under the following headings:

Experimental systematics: These were estimated by the same method as followed in Ref. [24]. The standard analysis using charged tracks and electromagnetic clusters was repeated using tracks only, or clusters only. A tighter cut on the direction of the thrust axis, constraining it to lie in the barrel part of the detector, was imposed, and the value of α_s re-evaluated. The detector corrections were recomputed using HERWIG [21] as the input to the detector simulation program, and again α_s was determined. The largest difference between any pair of α_s values was taken to define a systematic error. Finally, the changes in α_s when the fit range was altered (subject to the requirement that χ^2/d.o.f. should not be significantly worse than for the standard fits) were used to estimate a systematic error, which was combined in quadrature with the other experimental systematics.

Hadronization uncertainties: These were estimated by using different hadronization models or parameter sets to define the hadronization corrections. The same possibilities were considered as in Ref. [19], where a longer discussion is given. The changes in α_s under each variation in the hadronization model are listed in Table 3. The parameters of the JETSET 7.3 model [17] were determined from a fit to OPAL data on global event shapes [20]. This fit procedure yielded values of the parameters with some range of uncertainty, so we have independently varied the two parameters which are specifically related to hadronization, σ_q=`PARJ(21)`$=0.37^{+0.03}_{-0.05}$ GeV and a=`PARJ(41)`$=0.18^{+0.12}_{-0.05}$, by ± 1 standard deviation about their optimized values. The fragmentation function for heavy quarks was changed to the form proposed by Peterson et al. [31], using a set of fragmentation parameters [22] again derived by fitting OPAL data. An estimate of the influence of quark masses was made by performing the hadronization correction by excluding $\mathrm{b\overline{b}}$ events at the parton level, whilst including all flavours at the hadron level. In this way the corrected parton level distribution corresponds to u,d,s,c quarks only. The minimum value, Q_0, for the parton virtuality in JETSET was varied in the range 1 to 6 GeV. The HERWIG program [21] uses a cluster fragmentation model which is quite different from the string model [32] employed in JETSET. The ARIADNE model [23] uses a colour dipole formulation of the parton shower, with the standard Lund string model for hadronization. In order to be conservative in assigning the errors, we combine in quadrature all the contributions[‖] in Table 3 to define the total error.

Higher order effects: The standard approach is to use the variation of $\alpha_s(M_{Z^0})$ with x_μ to estimate the possible size of higher order effects. Following our other $\mathcal{O}(\alpha_s^2)$ analyses [19, 24, 25, 26] we take the values of $\alpha_s(M_{Z^0})$ for x_μ=1 and for x_μ fitted, average them to define the central value of $\alpha_s(M_{Z^0})$, and take half their difference to define the systematic error.

[‖] In the case of the variation of a and σ_q, the larger of the $+1$ s.d. and -1 s.d. changes was taken, as in Ref. [19].

In the case of $D_2(R)$ this yields a rather small uncertainty, yet the strong dependence of χ^2/d.o.f. on x_μ suggests that higher order effects are not unimportant for this observable. Nonetheless, for the sake of consistency with our other results, we follow our previously defined procedure. It may be noted that changing the value of Q_0 also provides some indication of higher order effects; a smaller value of Q_0 yields a larger parton multiplicity, and thus more of the higher order effects remain in the corrected parton level data. In fact $D_2(R)$ shows significant sensitivity to the choice of Q_0, and the results of Ref. [24] also suggest that the observables which are least sensitive to the choice of x_μ are generally most sensitive to Q_0.

Overlap treatment: In $\overline{\mathrm{p}}\mathrm{p}$ experiments significant uncertainties have arisen because of detailed differences between the jet definitions used in the experiments and in the QCD calculations, particularly in the handling of overlaps. This problem should be substantially alleviated in the present study, since we have applied the identical algorithm to the data and to integration of the $\mathcal{O}(\alpha_s^2)$ QCD matrix elements. To check this, we repeated the analysis changing from 0.75 to 0.5 the parameter f used in assigning particles in the regions between overlapping cones. This change was made both in generating the corrected data and in computing the QCD coefficients. The changes in the final values of $\alpha_s(M_{\mathrm{Z}^0})$ were found to be very small, though the dependence of $\alpha_s(M_{\mathrm{Z}^0})$ on x_μ was slightly weaker for $D_2(\varepsilon)$ when $f = 0.5$ was used.

Finally the different sources of uncertainty are combined in quadrature to provide the total errors quoted in Table 3. The measurements of $\alpha_s(M_{\mathrm{Z}^0})$ obtained from the two cone-jet variables:

$$\alpha_s(M_{\mathrm{Z}^0}) = 0.1188 \pm 0.0081$$

from $D_2(\varepsilon)$ and

$$\alpha_s(M_{\mathrm{Z}^0}) = 0.1160 \pm 0.0075$$

from $D_2(R)$, are compatible.

The new measurements may be combined with the $\mathcal{O}(\alpha_s^2)$ measurements from Ref. [19] in which systematic uncertainties were treated in the same way (except that in the present analysis we have one new source of uncertainty, connected with the overlap treatment). As in our previous papers [24, 19] we employ a simple weighted mean, in which we take due account of correlations between the systematic errors when assigning the systematic uncertainties on the mean. The result, based on 9 observables ($D_2(R)$, $D_2(\varepsilon)$, T, M_H, B_T, B_W, Σ_{EEC} and R_2 and $\mathcal{N}$ in the Durham scheme, where the last seven observables are defined in Ref. [19]), is:

$$\alpha_s(M_{\mathrm{Z}^0}) = 0.121 \pm 0.006 \quad .$$

For comparison, the OPAL global analysis of 13 observables in $\mathcal{O}(\alpha_s^2)$ in Ref. [24] yielded $\alpha_s(M_{\mathrm{Z}^0}) = 0.122^{+0.006}_{-0.005}$, while our similar analysis of 7 observables using combined $\mathcal{O}(\alpha_s^2)$+NLLA (resummed) QCD in Ref. [19] gave $\alpha_s(M_{\mathrm{Z}^0}) = 0.120 \pm 0.006$. The present analysis using cone jet rates has therefore provided new measurements of $\alpha_s(M_{\mathrm{Z}^0})$ which are compatible with previous measurements, and whose errors are competitive with the earlier results.

6 Energy flow within jets

6.1 Measurement of energy flow in e^+e^- jets

One important motivation for introducing a cone jet finder in e^+e^- studies was to facilitate the comparison of jet properties between e^+e^- and $\overline{p}p$ experiments. We have therefore measured the angular distribution of energy flow with respect to the axis of a jet. Measurements of this type have recently been published by the CDF collaboration [33], and compared with next-to-leading order QCD predictions. The cone jet finder was run on the same OPAL data sample as used in the measurement of α_s, using our canonical values R=0.7 rad and ε=7 GeV. The jet energies in an event were multiplied by a factor E_{cm}/E_{vis} in order to compensate roughly for undetected particles or particles unassigned to jets, for the double counting of energy between tracking and calorimetry, and for detector resolution. The average correction factor was 0.95. For the present analysis we required the jets to have energy greater than 35 GeV, which accepts most jets of energy close to the beam energy. The mean jet energy of this sample was 44.5 GeV, which is comparable with the transverse energy, E_T, of the CDF jets.

The energy flow was characterised by the "jet profile", $\psi(r)$, defined as the fraction of the energy of a jet lying within a smaller cone of half angle r, where the smaller cone has the same axis as the jet. The differential distribution $\Phi(r) = \frac{\psi(r+\Delta r)-\psi(r)}{\Delta r/R}$ was also measured. The bin size, $\Delta r/R$ was chosen to be the same as in the CDF analysis. The data were corrected for detector acceptance and resolution by the same method as used for the jet rates in Sect. 5. The corrections to $\psi(r)$ were small, less than 1%, while those to $\Phi(r)$ were less than 5% over most of the range of r. As before, experimental systematic errors were estimated using tracks and electromagnetic energy separately, and by using HERWIG instead of JETSET as the input to the detector simulation program when computing the detector corrections. A further source of systematic error could be the treatment of overlapping cones. This has been investigated by changing the value of ε; as ε is increased the number of proto-jets becomes smaller, and thus the likelihood of jets overlapping is reduced, while the number of jets above 35 GeV is essentially unaltered. This check therefore gives an indication of the possible influence of nearby jets. As ε was varied in the range 5 GeV$<\varepsilon<$25 GeV, the change in $\Phi(r)$ was found to be below 1% in most cases, though increasing with r, reaching about 8% for ε=25 GeV at $r/R \sim 1$. This variation of $\Phi(r)$ was included as an additional (asymmetric) source of systematic error. The measured values of $\Phi(r)$ and $\psi(r)$ for R =0.7 rad and for R =1.0 rad are given in Table 4.

6.2 Comparison with jets in $\overline{p}p$ interactions

In Figure 6 we show the dependence of $\psi(r)$ and $\Phi(r)$ on r/R for two values of R, 0.7 rad (our default) and 1.0 rad. We note that as R is increased from 0.7 to 1.0 rad, the jet energy is slightly more concentrated at small values of r/R, as expected. For comparison we show the measurements of the CDF experiment in $\overline{p}p$ interactions at 1800 GeV c.m. energy [33]. The CDF data correspond to a cone size R=1 rad, and transverse energy, E_T, between 40 and 60 GeV, with a mean of 45 GeV. The data show that the energy in the e^+e^- jets is concentrated closer to the jet axis, with a corresponding depletion at large angles. In other words, the LEP jets are narrower than those observed in $\overline{p}p$ collisions. For example, for R = 1.0 rad, the

e^+e^- jets show $52 \pm 1\%$ of the energy in $r/R < 0.1$ and $7.6 \pm 0.3\%$ in $r/R > 0.5$, while the corresponding fractions in $\overline{p}p$ are $27 \pm 3\%$ and $19.5 \pm 1.5\%$ respectively.

There are still some residual differences between the cone jet finding algorithms used by OPAL and CDF. These differences arise because the centre-of-mass of the hard collision is in general boosted in the laboratory frame in hadron collisions. For this reason, in hadron colliders the jets are defined by $\sqrt{\Delta\eta^2 + \Delta\phi^2} < R$, where the pseudorapidity $\eta = -\ln(\tan\frac{\theta}{2})$, $\Delta\eta$ and $\Delta\phi$ are the differences between the cone axis and a particle direction, and ϕ and θ are the usual spherical polar angles, ϕ being measured in radians. This procedure approximates a cone in the centre-of-mass of the hard collision, while in e^+e^- we can define such a cone directly in the laboratory system. Similarly, in hadron collisions the transverse energy, $E_T = E\sin\theta$, is used because it is independent of the longitudinal boost of the hard scatter, where in e^+e^- the use of E is more natural. We shall refer to the CDF algorithm as the "E_T-η-ϕ" metric, to contrast it with our standard algorithm operating in the "E-χ" metric, χ being the angle between a particle and the jet axis.

The cone definitions in η-ϕ space and in terms of χ should be equivalent near to $\theta = 90°$, but differ significantly near the beam directions – in particular an η-ϕ cone can never encompass the beam axis, while the simple E-χ cone may. However, experimental considerations have led to the CDF data being restricted to cone axes lying within $0.1 < |\eta| < 0.7$, and in this region the differences between the two metrics should be small. Furthermore, the CDF jet profiles are measured using $E_T = E\sin\theta$, while the OPAL data use E. To assess the effect of these differences, we have reanalysed the OPAL data using procedures identical to CDF, i.e. defining the cone in the η-ϕ metric, demanding $|\eta| < 0.7$ and measuring the energy flow in terms of E_T. The resulting jet profiles are given in Table 5, and compared with the CDF data in Fig. 7. The e^+e^- jet profiles became somewhat broader when the E_T-η-ϕ metric was used, but this change was almost entirely eliminated once the $|\eta| < 0.7$ cut was imposed. The net effect of all three changes to the algorithm was to increase $\Phi(r)$ by up to 4% in $0.1 < r/R < 0.6$, and to reduce $\Phi(r)$ by between 2% and 8% in the other regions. These changes to the algorithm are clearly unable to explain the differences between the e^+e^- and $\overline{p}p$ jets.

Another difference between the e^+e^- and $\overline{p}p$ data is that the CDF jets have slightly higher energy than the OPAL jets, since the average E_T in CDF is roughly equal to the average E in OPAL. In fact, the OPAL jet sample has average E_T ~40.4 GeV after making the $|\eta| < 0.7$ cut. This would, however, act in the wrong direction to explain the discrepancy, since the jet profiles are known to become narrower with increasing jet energy [33]. If the OPAL data are subjected to a cut $E_T > 35$ GeV instead of $E > 35$ GeV, the jet profiles become significantly narrower, thus increasing the difference from the CDF measurements. However, such a cut does not really make sense in the e^+e^- case, because the maximum jet energy is bounded by the beam energy, and so a cut on E_T represents a bias towards the highest energy jets, which are those which have undergone the least gluon radiation.

A further, more general, difference between e^+e^- and $\overline{p}p$ interactions which could affect the jet profiles is the presence of an underlying event in $\overline{p}p$. The underlying event is understood to consist of particles resulting from the fragmentation of those remnants of the colliding hadrons which did not participate in the hard scatter. An estimate of the contribution of the underlying event has been made by measuring the energy in cones of size $R = 0.7$ rad at 90° to the scattered jets in the CDF data at 1800 GeV c.m. energy [34]. A value of 1.5 GeV is found, with errors

$^{+30}_{-50}$%, where the lower error corresponds to the energy seen in "minimum bias" events. Slightly higher values for the E_T density are quoted in Ref. [35]: 0.7 GeV/R^2 in minimum bias events and 1.6 GeV/R^2 in jet events**. It may however be argued [35] that the value derived from jet events is too high, since it includes energy associated with the jets which is emitted outside their cones, often referred to as "splash-out". To assess the possible effect of the underlying event on the comparison with e^+e^- jets, we have corrected the CDF data by subtracting a uniform underlying distribution of energy, and then renormalizing the corrected $\Phi(r)$ so that $\int_0^R \Phi(r)dr/R = 1$. In Fig. 8 we repeat the comparison shown in Fig. 7, after correcting the CDF data for underlying densities 0.7 GeV/R^2 and 1.6 GeV/R^2. Clearly the underlying event accounts for part of the difference between the e^+e^- and $\overline{p}p$ jets, but even taking the (probably overestimated) density of 1.6 GeV/R^2 a substantial discrepancy remains (for example, using 1.6 GeV/R^2 the corrected CDF jet profile would show 30 ± 3% of the energy in $r/R < 0.1$ and 12.5 ± 1.5% in $r/R > 0.5$, compared with 51 ± 1% and 7.0 ± 0.3% respectively in e^+e^-).

Since the e^+e^- data have no underlying event, it is possible to investigate the "splash-out" flow of energy outside the jet cones. We take events, apply the cone jet finder with $R = 0.7$ rad and ε=7 GeV using the E-χ metric, and define the event axis to be the axis of the most energetic jet. We then measure the fractional energy flow per unit solid angle, $1/E_{cm}dE/d\Omega$, as a function of the angle χ to the jet axis. The data are corrected for acceptance and detector resolution, and systematic errors estimated, in the same way as for the jet profiles. The results are shown in Table 6. In Fig. 9 we show these measurements, both for an inclusive event sample, and also for two-jet events. The step in the distribution around 40° corresponds to the edge of the $R = 0.7$ rad cone used in the jet finder; in most cases the algorithm is likely by a small change of the jet axis to include a particle lying just outside a cone. The asymmetry about 90° in the inclusive sample arises because gluon emission is most likely in the hemisphere opposite the most energetic jet; it is largely reduced in the two-jet sample. From these data we may, for example, estimate the energy in a cone of size $R = 0.7$ rad at 90° to the event axis to be 0.5 GeV in two-jet events and 0.9 GeV in the inclusive sample. These results for splash-out from a fragmenting quark-antiquark system may be compared with the 1.5 GeV (splash-out and underlying event) observed in jet events at CDF.

Since differences between the algorithms, or the underlying event, are unable to explain the differences between the e^+e^- and $\overline{p}p$ data, the effect may signify some difference in the QCD dynamics of the two environments. For example, in $\overline{p}p$ there are processes, such as initial state gluon radiation and colour flows connecting initial and final partons, which have no counterparts in e^+e^-. Perhaps more importantly, the jets in the OPAL study, which have been constrained to lie close to the beam energy, are predominantly quark jets (3.4 ± 0.3% are gluon jets, as determined from Monte Carlo studies) while most of the jets in the CDF sample are expected to be induced by gluons (based on the HERWIG Monte Carlo [21] we estimate around 75% to be gluon-induced). Because of the greater colour charge of the gluon, more radiation may be expected from gluons than from quarks, leading to broader gluon jets.

In previous OPAL publications [22, 36] we studied differences between quark and gluon jets, using three-jet events with a two-fold symmetric topology in which the two lower energy jets made angles of $\sim 150°$ with the third jet. By tagging a heavy flavour decay in one of the two lower energy jets, a clean sample of gluon jets having energy around 24 GeV could be identified,

**The notation GeV/R^2 is understood to refer to the E_T density per unit area in η-ϕ space, so that a cone of half-angle R corresponds to an area πR^2.

and compared with an unbiased sample of quark jets of the same energy and in the same event environment. In particular, the observed differences between the jet profiles in tagged gluon and quark jets closely resemble the differences between $\overline{\mathrm{p}}\mathrm{p}$ and $\mathrm{e}^+\mathrm{e}^-$ seen in Fig. 8 (compare Fig. 8 in the present paper with Fig. 13a of Ref. [22]). However, there are some detailed differences between the analysis of Ref. [22] and the present study, which should be borne in mind in making comparisons. By virtue of the kinematic selection of events, the jets in Ref. [22] have a lower energy than those studied in $\overline{\mathrm{p}}\mathrm{p}$ and in the present $\mathrm{e}^+\mathrm{e}^-$ data, and it was not possible to study the jet profiles over the full range $R < 1$ rad because the jets would overlap, being only 60° apart. Also, the jets in Ref. [22] were defined using the Durham jet finding algorithm, and the data were not corrected for detector acceptance and resolution, though these differences do not significantly affect the present comparison. Nonetheless, the striking resemblance between the differences in the jet profiles in tagged quark and gluon jets at $E \sim 24$ GeV in Ref. [22] and the differences we observe between $\overline{\mathrm{p}}\mathrm{p}$ and $\mathrm{e}^+\mathrm{e}^-$ data at ~ 45 GeV suggests that most of the difference between the $\overline{\mathrm{p}}\mathrm{p}$ and $\mathrm{e}^+\mathrm{e}^-$ data can be ascribed to differences between quark and gluon jet properties. With increasing LEP statistics, samples of tagged gluon jets at close to 45 GeV, well separated from the quark jets, can eventually be obtained [37], which will permit a more direct comparison between gluon jets in $\mathrm{e}^+\mathrm{e}^-$ collisions and the CDF data.

7 Discussion and Summary

In this paper we have introduced a jet finding algorithm for $\mathrm{e}^+\mathrm{e}^-$ interactions which closely resembles the cone-based jet finders typically used in $\overline{\mathrm{p}}\mathrm{p}$ experiments. We have compared the performance of the cone algorithm with the invariant mass (JADE-type) algorithms which have become standard in most $\mathrm{e}^+\mathrm{e}^-$ analyses. The jets produced by the algorithms differ in several important respects, but we find that the overall performance of the cone scheme is broadly similar to the JADE-type schemes. By comparing jets found at the parton, hadron, and detector levels in Monte Carlo events, we find that the cone algorithm provides better angular resolution and generally somewhat better energy resolution. However, the effects of hadronization on the numbers of jets found are greater for the cone jets. Thus the cone jet finder provides a useful alternative to the established JADE-type algorithms. In particular, analyses which rely on good estimation of the direction of a jet (to estimate a parent hadron's or parton's direction for example) should benefit from the use of the cone algorithm. In three-jet events, the jet energies can be best estimated by using the angles between the jets, so that the good angular resolution of cone jets will be useful. The cone jet finder should also prove beneficial in any analysis in which it is desired to exclude particles far in angle from the jet axis, e.g. the study of differences between quark and gluon jets, where the assignment of particles far from the jet axes may be ambiguous. Further discussion may be found in Ref. [16].

We have measured jet rates using the cone jet finder as a function of the two parameters which govern the algorithm, the cone half-angle R and the minimum jet energy ε. These measurements have been compared with the predictions of $\mathcal{O}(\alpha_s^2)$ QCD. We find that the data can be satisfactorily described by QCD, but only if the renormalization scale factor x_μ is optimized by fitting to the data. These comparisons have permitted us to make two new measurements of the strong coupling constant, $\alpha_s(M_{\mathrm{Z}^0})$. The results obtained:

$$\alpha_s(M_{\mathrm{Z}^0}) = 0.119 \pm 0.008$$

from the dependence of jet rates on minimum jet energy and

$$\alpha_s(M_{\mathrm{Z}^0}) = 0.116 \pm 0.008$$

from their dependence on cone size, are compatible with previous measurements, and yield errors which are competitive with the previously studied observables. Combining with other recent OPAL measurements using $\mathcal{O}(\alpha_s^2)$ QCD we obtain:

$$\alpha_s(M_{\mathrm{Z}^0}) = 0.121 \pm 0.006 \quad .$$

One of the original reasons for implementing a cone-based jet finder in $\mathrm{e^+e^-}$ interactions was to facilitate comparisons between the properties of jets formed in $\mathrm{e^+e^-}$ and $\mathrm{\overline{p}p}$ collisions. We have therefore compared the energy profiles, i.e. the energy flow with respect to the jet axis, for our measurements of jets at $E \sim 45$ GeV with recent CDF data for jets having $E_T \sim 45$ GeV. We find that the jets in $\mathrm{e^+e^-}$ are substantially narrower than those observed in $\mathrm{\overline{p}p}$ interactions. Small remaining differences between the jet finding algorithms have been investigated, and are unable to account for the discrepancy. The influence of the underlying event in the $\mathrm{\overline{p}p}$ case has been studied, and proves to explain only a small part of the differences seen. Thus a dynamical explanation must be sought; for example, the jets in the OPAL data are mostly induced by quarks, whilst those in the CDF data are largely gluon induced. Analogous differences between quark and gluon jet fragmentation observed by OPAL in Ref. [22] for ~ 24 GeV jets, suggest that these are responsible for a major part of the observed discrepancy.

Acknowledgements

We thank S. Ellis for valuable discussions concerning parts of this analysis, and D.E. Soper and H-C. Yang for providing jet finding code which served as a starting point for this work. We also thank the CDF collaboration (in particular J. Huth) for help in supplying numerical values of the CDF data.

It is a pleasure to thank the SL Division for the efficient operation of the LEP accelerator, the precise information on the absolute energy, and their continuing close cooperation with our experimental group. In addition to the support staff at our own institutions we are pleased to acknowledge the
Department of Energy, USA,
National Science Foundation, USA,
Texas National Research Laboratory Commission, USA,
Science and Engineering Research Council, UK,
Natural Sciences and Engineering Research Council, Canada,
Fussefeld Foundation,
Israeli Ministry of Energy and Ministry of Science,
Minerva Gesellschaft,
Japanese Ministry of Education, Science and Culture (the Monbusho) and a grant under the Monbusho International Science Research Program,
German Israeli Bi-national Science Foundation (GIF),
Direction des Sciences de la Matière du Commissariat à l'Energie Atomique, France,
Bundesministerium für Forschung und Technologie, Germany,
National Research Council of Canada,
A.P. Sloan Foundation and Junta Nacional de Investigação Científica e Tecnológica, Portugal.

References

[1] JADE Collaboration, W. Bartel et al., Z. Phys. **C33** (1986) 23;
JADE Collaboration, S. Bethke et al., Phys. Lett. **B213** (1988) 235.

[2] S. Bethke, Z. Kunszt, D. E. Soper and W.J. Stirling, Nucl. Phys. **B370** (1992) 310.

[3] N. Brown and W.J. Stirling, Z. Phys. **C53** (1992) 629.

[4] S. Catani et al., Phys. Lett. **B269** (1991) 432.

[5] UA1 Collaboration, G. Arnison et al., Phys. Lett. **123B** (1983) 115.

[6] CDF Collaboration, F. Abe et al., Phys. Rev. **D45** (1992) 1448.

[7] G. Sterman and S. Weinberg, Phys. Rev. Lett. **39** (1977) 1436.

[8] J.E. Huth et al., *Research Directions for the Decade*, Snowmass (1990), 134. (Ed. E.L. Berger; World Scientific, Singapore).

[9] H.J. Daum, H. Meyer and J. Bürger, Z. Phys. **C8** (1981) 167;
PLUTO Collaboration, Ch. Berger et al., Phys. Lett. **97B** (1980) 459;
JADE Collaboration, W. Bartel et al., Phys. Lett. **119B** (1982) 239.

[10] OPAL Collaboration, K. Ahmet et al., Nucl. Instr. and Meth. **A305** (1991) 275.

[11] P.P. Allport et al., Nucl. Instr. and Meth. **A324** (1993) 34.

[12] M. Arignon et al., Nucl. Instr. and Meth. **A313** (1992) 103.

[13] D.G. Charlton, F. Meijers, T.J. Smith and P.S. Wells, Nucl. Instr. and Meth. **A325** (1993) 129.

[14] OPAL Collaboration, G. Alexander et al., Z. Phys. **C52** (1991) 175.

[15] S. Brandt et al., Phys. Lett. **12** (1964) 57;
E. Farhi, Phys. Rev. Lett. **39** (1977) 1587.

[16] L.A. del Pozo, Ph. D. Thesis, University of Cambridge (December 1993), RALT-002.

[17] T. Sjöstrand, Comp. Phys. Commun. **39** (1986) 347;
T. Sjöstrand, Comp. Phys. Commun. **43** (1987) 367;
M. Bengtsson and T. Sjöstrand, Nucl. Phys. **B289** (1987) 810.

[18] J. Allison et al., Nucl. Instr. and Meth. **A317** (1992) 47.

[19] OPAL Collaboration, P.D. Acton et al., Z. Phys. C. **C59** (1993) 1.

[20] OPAL Collaboration, M.Z. Akrawy et al., Z. Phys. **C47** (1990) 505.

[21] G. Marchesini and B.R. Webber, Nucl. Phys. **B310** (1988) 461;
G. Marchesini et al. Comp. Phys. Commun. **67** (1992) 465.

[22] OPAL Collaboration, P.D. Acton et al., Z. Phys. C. **C58** (1993) 387.

[23] U. Pettersson, LU TP 88-5 (1988);
L. Lönnblad and U. Pettersson, LU TP 88-15 (1988);
L. Lönnblad, LU TP 89-10 (1988).

[24] OPAL Collaboration, P.D. Acton et al., Z. Phys. **C55** (1992) 1.

[25] OPAL Collaboration, M.Z. Akrawy et al., Phys. Lett. **B235** (1990) 389.

[26] OPAL Collaboration, M.Z. Akrawy et al., Z. Phys. **C49** (1991) 375.

[27] Particle Data Group, K. Hikasa et al., *Review of Particle Properties*, Phys. Rev. **D45** (1992) III.54.

[28] W.A. Bardeen et al., Phys. Rev. **D18** (1978) 3998.

[29] Z.Kunszt and P.Nason [conv.], in "Z Physics at LEP 1" (eds. G.Altarelli, R.Kleiss and C.Verzegnassi), CERN 89-08 (1989).

[30] R.K. Ellis, D.A. Ross and A.E. Terrano, Nucl. Phys. **B178** (1981) 421.

[31] C. Peterson, D. Schlatter, I. Schmitt and P.M. Zerwas, Phys. Rev. **D27** (1983) 105.

[32] B. Andersson, G. Gustafson, G. Ingelman and T. Sjöstrand, Phys. Rep. **97** (1983) 31.

[33] CDF Collaboration, F. Abe et al., Phys. Rev. Lett. **70** (1993) 713.

[34] CDF Collaboration, F. Abe et al., Phys. Rev. Lett. **70** (1993) 1376.

[35] S.D. Ellis, in proceedings of XXVIIIth Rencontres de Moriond, CERN TH-6861/93 (1993).

[36] OPAL Collaboration, G. Alexander et al., Phys. Lett. **B265** (1991) 462.

[37] J.W. Gary, Preprint UCRHEP-T116; to be published in Phys. Rev. D.

ε/ GeV	R_2	R_3	R_4
3	61.22 ± 0.14 ± 1.00	28.84 ± 0.13 ± 0.81	8.26 ± 0.07 ± 0.46
5	69.55 ± 0.10 ± 1.00	24.98 ± 0.09 ± 0.77	4.86 ± 0.07 ± 0.28
7	74.69 ± 0.12 ± 0.96	21.90 ± 0.12 ± 0.66	3.15 ± 0.05 ± 0.21
9	78.79 ± 0.09 ± 1.00	19.08 ± 0.10 ± 0.70	1.97 ± 0.05 ± 0.14
12	83.92 ± 0.08 ± 0.91	15.10 ± 0.08 ± 0.54	0.87 ± 0.03 ± 0.08
15	88.30 ± 0.08 ± 1.04	11.29 ± 0.08 ± 0.59	0.27 ± 0.01 ± 0.04
18	92.34 ± 0.08 ± 1.01	7.46 ± 0.08 ± 0.47	0.03 ± 0.01 ± 0.01
21	95.82 ± 0.06 ± 1.12	3.87 ± 0.05 ± 0.24	—
25	98.04 ± 0.06 ± 1.44	0.61 ± 0.02 ± 0.08	—
R / rad	R_2	R_3	R_4
0.3	62.23 ± 0.10 ± 1.63	28.36 ± 0.12 ± 0.50	7.94 ± 0.08 ± 0.42
0.5	68.74 ± 0.11 ± 1.21	25.30 ± 0.12 ± 0.72	5.19 ± 0.07 ± 0.38
0.7	74.69 ± 0.12 ± 0.96	21.90 ± 0.12 ± 0.66	3.15 ± 0.05 ± 0.21
0.9	81.03 ± 0.07 ± 0.48	17.57 ± 0.08 ± 0.35	1.35 ± 0.03 ± 0.12
1.1	87.71 ± 0.07 ± 0.25	11.99 ± 0.08 ± 0.16	0.29 ± 0.02 ± 0.02
1.3	94.87 ± 0.04 ± 0.18	5.08 ± 0.04 ± 0.05	0.03 ± 0.01 ± 0.01
1.5	99.47 ± 0.02 ± 0.10	0.54 ± 0.02 ± 0.02	—

Table 1: Measured jet production rates (in % of all hadronic events) as the minimum jet energy ε is varied for fixed R=0.7 rad, and as R is varied for fixed ε=7 GeV. The data are corrected for detector resolution and acceptance. The first error is statistical, and the second shows the experimental systematic uncertainties.

		$D_2(\varepsilon)$	$D_2(R)$
$x_\mu = 1$:	$\alpha_s(M_{Z^0})$	0.1262	0.1165
	$\Lambda_{\overline{MS}}$ (MeV)	347 ± 8	207 ± 5
	χ^2/d.o.f.	26.3	182.2
x_μ fitted :	$\alpha_s(M_{Z^0})$	0.1113	0.1154
	$\Lambda_{\overline{MS}}$ (MeV)	151 ± 3	195 ± 5
	x_μ	0.067 ± 0.007	0.172 ± 0.005
	χ^2/d.o.f.	2.9	1.0

Table 2: Values of $\alpha_s(M_{Z^0})$, $\Lambda_{\overline{MS}}$, χ^2/d.o.f. and x_μ derived by fitting the QCD calculations to the data.

	$D_2(\varepsilon)$	$D_2(R)$
$\alpha_s(M_{Z^0})$	**0.1188**	**0.1160**
Statistical error	$\pm$0.0004	$\pm$0.0004
Experimental Syst.	$\pm$0.0017	$\pm$0.0026
Fit range variation	$\pm$0.0011	$^{+0.0015}_{-0.0020}$
JETSET $a+1$ s.d.	$+$0.0008	$+$0.0009
JETSET $a-1$ s.d.	$-$0.0005	$-$0.0005
JETSET $\sigma+1$ s.d.	$+$0.0001	$+$0.0002
JETSET $\sigma-1$ s.d.	$-$0.0002	$-$0.0004
JETSET /Peterson	$-$0.0008	$-$0.0011
JETSET udsc only	$+$0.0005	$+$0.0022
JETSET $Q_0 = 6$ GeV	$-$0.0012	$+$0.0060
HERWIG 5.5	$-$0.0009	$-$0.0012
ARIADNE 3.1	$-$0.0011	$+$0.0002
Total Hadronization	$\pm$0.0022	$\pm$0.0067
x_μ variation	$\pm$0.0075	$\pm$0.0006
Overlap	$+$0.0002	$+$0.0005
Total Error	$\pm$**0.0081**	$\pm$**0.0075**

Table 3: The central values of $\alpha_s(M_{Z^0})$ derived from each of the cone jet observables (representing averages of fits with x_μ=1 and x_μ fitted), together with the different contributions to their errors. In the cases where a signed value is quoted, this indicates the direction in which $\alpha_s(M_{Z^0})$ changes with respect to the default analysis when a certain feature of the analysis is changed.

$R = 0.7$ rad and ε=7 GeV.

r/R	$\Phi(r)$	stat	expt	overlap	r/R	$\psi(r)$	stat	expt	overlap
0.0 – 0.1	4.351	±0.006	±0.121	$^{+0.004}_{-0.037}$	0.1	0.4351	±0.0006	±0.0121	$^{+0.0004}_{-0.0037}$
0.1 – 0.2	2.618	±0.003	±0.043	$^{+0.009}_{-0.002}$	0.2	0.6969	±0.0005	±0.0083	$^{+0.0003}_{-0.0033}$
0.2 – 0.3	1.171	±0.003	±0.013	$^{+0.004}_{-0.000}$	0.3	0.8140	±0.0002	±0.0058	$^{+0.0003}_{-0.0029}$
0.3 – 0.4	0.632	±0.001	±0.014	$^{+0.004}_{-0.000}$	0.4	0.8772	±0.0002	±0.0036	$^{+0.0003}_{-0.0025}$
0.4 – 0.5	0.389	±0.001	±0.010	$^{+0.003}_{-0.000}$	0.5	0.9161	±0.0002	±0.0021	$^{+0.0003}_{-0.0021}$
0.5 – 0.6	0.272	±0.001	±0.007	$^{+0.001}_{-0.000}$	0.6	0.9433	±0.0001	±0.0012	$^{+0.0003}_{-0.0020}$
0.6 – 0.7	0.200	±0.001	±0.004	$^{+0.003}_{-0.000}$	0.7	0.9633	±0.0001	±0.0008	$^{+0.0003}_{-0.0017}$
0.7 – 0.8	0.152	±0.001	±0.004	$^{+0.003}_{-0.000}$	0.8	0.9785	±0.0001	±0.0003	$^{+0.0002}_{-0.0014}$
0.8 – 0.9	0.120	±0.001	±0.002	$^{+0.006}_{-0.001}$	0.9	0.9905	±0.0001	±0.0001	$^{+0.0001}_{-0.0008}$
0.9 – 1.0	0.095	±0.001	±0.002	$^{+0.008}_{-0.001}$	1.0	1.0000	–	–	–

$R = 1.0$ rad and ε=7 GeV.

r/R	$\Phi(r)$	stat	expt	overlap	r/R	$\psi(r)$	stat	expt	overlap
0.0 – 0.1	5.163	±0.005	±0.110	$^{+0.005}_{-0.053}$	0.1	0.5163	±0.0005	±0.0110	$^{+0.0005}_{-0.0053}$
0.1 – 0.2	2.287	±0.004	±0.027	$^{+0.006}_{-0.001}$	0.2	0.7450	±0.0003	±0.0082	$^{+0.0004}_{-0.0047}$
0.2 – 0.3	0.943	±0.002	±0.021	$^{+0.012}_{-0.000}$	0.3	0.8393	±0.0003	±0.0049	$^{+0.0004}_{-0.0034}$
0.3 – 0.4	0.518	±0.001	±0.014	$^{+0.006}_{-0.000}$	0.4	0.8911	±0.0003	±0.0030	$^{+0.0004}_{-0.0028}$
0.4 – 0.5	0.333	±0.001	±0.008	$^{+0.002}_{-0.000}$	0.5	0.9244	±0.0002	±0.0020	$^{+0.0004}_{-0.0027}$
0.5 – 0.6	0.236	±0.001	±0.007	$^{+0.000}_{-0.000}$	0.6	0.9480	±0.0002	±0.0013	$^{+0.0004}_{-0.0027}$
0.6 – 0.7	0.180	±0.001	±0.004	$^{+0.002}_{-0.000}$	0.7	0.9660	±0.0001	±0.0008	$^{+0.0003}_{-0.0024}$
0.7 – 0.8	0.141	±0.001	±0.005	$^{+0.004}_{-0.001}$	0.8	0.9801	±0.0001	±0.0004	$^{+0.0003}_{-0.0020}$
0.8 – 0.9	0.112	±0.001	±0.003	$^{+0.008}_{-0.001}$	0.9	0.9913	±0.0001	±0.0001	$^{+0.0002}_{-0.0012}$
0.9 – 1.0	0.087	±0.001	±0.001	$^{+0.012}_{-0.002}$	1.0	1.0000	–	–	–

Table 4: Measured values for the differential and integral jet energy profiles, $\Phi(r)$ and $\psi(r)$, for R=0.7 rad and ε=7 GeV, and for R=1.0 rad and ε=7 GeV, using the E-χ metric. The data are corrected to the hadron level, and the sources of statistical and systematic error are quoted separately. The uncertainty associated with varying the treatment of overlapping cones, as described in the text, is listed separately.

r/R	$\Phi(r)$	stat	expt	overlap	r/R	$\psi(r)$	stat	expt	overlap
0.0 – 0.1	5.100	$\pm$0.008	$\pm$0.126	$^{+0.003}_{-0.034}$	0.1	0.5100	$\pm$0.0008	$\pm$0.0126	$^{+0.0003}_{-0.0034}$
0.1 – 0.2	2.378	$\pm$0.004	$\pm$0.040	$^{+0.006}_{-0.000}$	0.2	0.7478	$\pm$0.0005	$\pm$0.0086	$^{+0.0002}_{-0.0032}$
0.2 – 0.3	0.977	$\pm$0.003	$\pm$0.025	$^{+0.002}_{-0.000}$	0.3	0.8455	$\pm$0.0004	$\pm$0.0050	$^{+0.0002}_{-0.0030}$
0.3 – 0.4	0.524	$\pm$0.001	$\pm$0.010	$^{+0.003}_{-0.000}$	0.4	0.8979	$\pm$0.0003	$\pm$0.0034	$^{+0.0003}_{-0.0027}$
0.4 – 0.5	0.326	$\pm$0.002	$\pm$0.009	$^{+0.007}_{-0.000}$	0.5	0.9305	$\pm$0.0003	$\pm$0.0022	$^{+0.0002}_{-0.0020}$
0.5 – 0.6	0.227	$\pm$0.001	$\pm$0.007	$^{+0.002}_{-0.000}$	0.6	0.9532	$\pm$0.0002	$\pm$0.0014	$^{+0.0002}_{-0.0018}$
0.6 – 0.7	0.167	$\pm$0.001	$\pm$0.004	$^{+0.003}_{-0.000}$	0.7	0.9699	$\pm$0.0001	$\pm$0.0010	$^{+0.0002}_{-0.0015}$
0.7 – 0.8	0.127	$\pm$0.001	$\pm$0.005	$^{+0.003}_{-0.000}$	0.8	0.9826	$\pm$0.0001	$\pm$0.0005	$^{+0.0002}_{-0.0012}$
0.8 – 0.9	0.099	$\pm$0.001	$\pm$0.002	$^{+0.005}_{-0.001}$	0.9	0.9925	$\pm$0.0001	$\pm$0.0002	$^{+0.0001}_{-0.0006}$
0.9 – 1.0	0.075	$\pm$0.001	$\pm$0.003	$^{+0.006}_{-0.001}$	1.0	1.0000	–	–	–

Table 5: Measured values for the differential and integral jet energy profiles, $\Phi(r)$ and $\psi(r)$, for R=1.0 rad and ε=7 GeV. The algorithm was modified to emulate exactly the CDF procedure, i.e. defining the cone in the η-ϕ metric, demanding $|\eta| < 0.7$ and measuring the energy flow in terms of E_T. The data are corrected to the hadron level, and the sources of statistical and systematic error are quoted separately. The uncertainty associated with varying the treatment of overlapping cones, as described in the text, is listed separately.

	Inclusive	Two-jet events
χ / deg	$1/E_{cm}\,dE/d\Omega$	$1/E_{cm}\,dE/d\Omega$
0 – 4	11.80 ± 0.54	12.16 ± 0.55
4 – 8	2.63 ± 0.05	2.70 ± 0.06
8 – 12	0.773 ± 0.012	0.798 ± 0.010
12 – 16	0.321 ± 0.010	0.335 ± 0.011
16 – 20	0.163 ± 0.006	0.171 ± 0.006
20 – 24	0.095 ± 0.004	0.100 ± 0.005
24 – 28	0.060 ± 0.002	0.064 ± 0.003
28 – 32	0.0400 ± 0.0017	0.0417 ± 0.0021
32 – 36	0.0300 ± 0.0007	0.0289 ± 0.0007
36 – 40	0.0199 ± 0.0005	0.0205 ± 0.0005
40 – 44	0.0064 ± 0.0001	0.0057 ± 0.0001
44 – 48	0.0066 ± 0.0001	0.0055 ± 0.0002
48 – 52	0.0055 ± 0.0002	0.0045 ± 0.0002
52 – 56	0.0049 ± 0.0001	0.0039 ± 0.0002
56 – 60	0.0044 ± 0.0002	0.0035 ± 0.0002
60 – 64	0.0041 ± 0.0001	0.0032 ± 0.0001
64 – 68	0.0038 ± 0.0002	0.0030 ± 0.0001
68 – 72	0.0038 ± 0.0001	0.0029 ± 0.0001
72 – 76	0.0039 ± 0.0001	0.0028 ± 0.0001
76 – 80	0.0039 ± 0.0002	0.0029 ± 0.0001
80 – 84	0.0042 ± 0.0001	0.0028 ± 0.0001
84 – 88	0.0044 ± 0.0003	0.0029 ± 0.0001
88 – 92	0.0050 ± 0.0001	0.0030 ± 0.0001
92 – 96	0.0056 ± 0.0001	0.0032 ± 0.0001
96 – 100	0.0065 ± 0.0001	0.0034 ± 0.0001
100 – 104	0.0076 ± 0.0002	0.0036 ± 0.0001
104 – 108	0.0088 ± 0.0004	0.0040 ± 0.0001
108 – 112	0.0104 ± 0.0004	0.0044 ± 0.0001
112 – 116	0.0125 ± 0.0004	0.0049 ± 0.0002
116 – 120	0.0146 ± 0.0004	0.0056 ± 0.0003
120 – 124	0.0175 ± 0.0005	0.0065 ± 0.0004
124 – 128	0.0206 ± 0.0006	0.0078 ± 0.0003
128 – 132	0.0243 ± 0.0006	0.0094 ± 0.0003
132 – 136	0.0289 ± 0.0003	0.0122 ± 0.0004
136 – 140	0.0349 ± 0.0006	0.0153 ± 0.0006
140 – 144	0.0385 ± 0.0003	0.0148 ± 0.0005
144 – 148	0.0459 ± 0.0005	0.0176 ± 0.0009
148 – 152	0.0588 ± 0.0008	0.0250 ± 0.0014
152 – 156	0.0805 ± 0.0012	0.0383 ± 0.0020
156 – 160	0.1200 ± 0.0013	0.0663 ± 0.0005
160 – 164	0.1956 ± 0.0020	0.1306 ± 0.0026
164 – 168	0.364 ± 0.006	0.311 ± 0.006
168 – 172	0.828 ± 0.014	0.916 ± 0.012
172 – 176	2.44 ± 0.03	3.14 ± 0.09
176 – 180	8.64 ± 0.27	11.47 ± 0.50

Table 6: Measured values for the energy flow per unit solid angle, $1/E_{cm}\,dE/d\Omega$, for an inclusive sample of events, and for two-jet events. The errors include statistical and systematic experimental uncertainties.

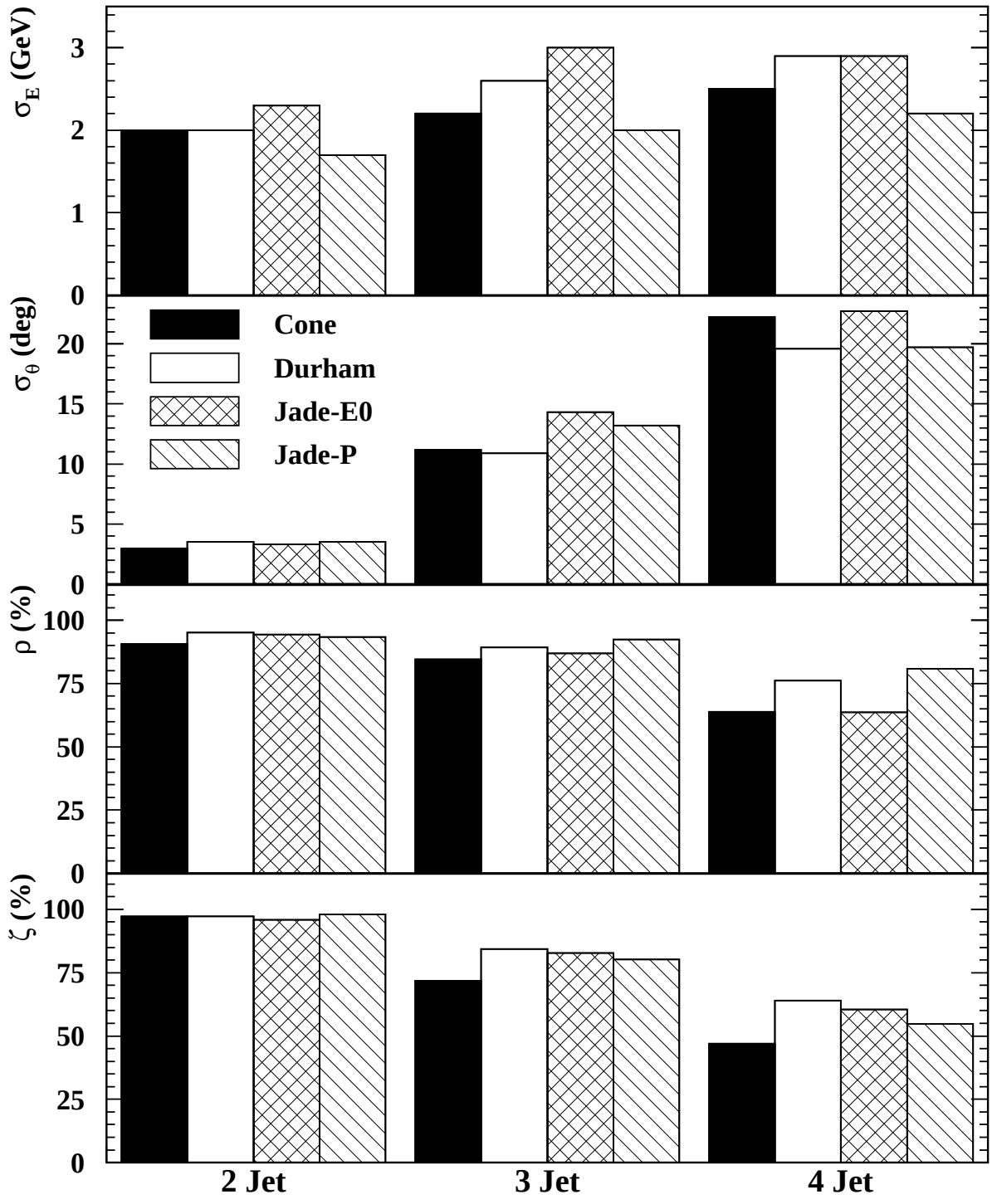

Figure 1: Comparison of energy and angular resolutions and jet number purities and efficiencies for different jet finders. These are based on comparisons between jets at the hadron and parton levels, and thus provide a measure of hadronization effects. The parameters for the cone algorithm were R=0.7 rad and ε=7 GeV, the JADE-E0 jet finder was run with y_{cut}=0.06, the JADE-p jet finder with y_{cut}=0.05 and the Durham scheme with y_{cut}=0.02.

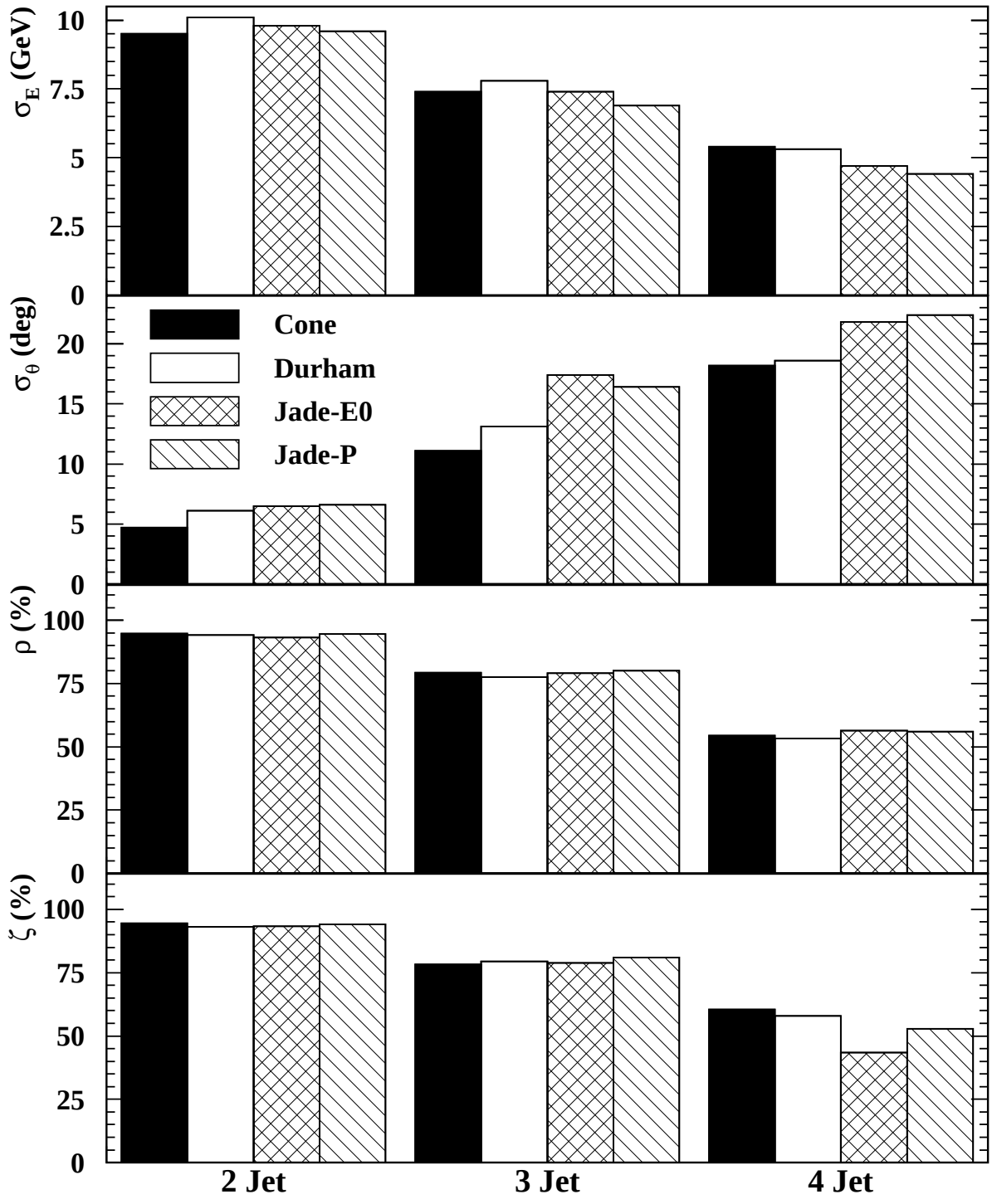

Figure 2: Comparison of energy and angular resolutions and jet number purities and efficiencies for different jet finders. These are based on comparisons between jets at the detector and hadron levels, and thus provide a measure of detector effects. The parameters for the cone algorithm were R=0.7 rad and ε=7 GeV, the JADE-E0 jet finder was run with y_{cut}=0.06, the JADE-p jet finder with y_{cut}=0.05 and the Durham scheme with y_{cut}=0.02.

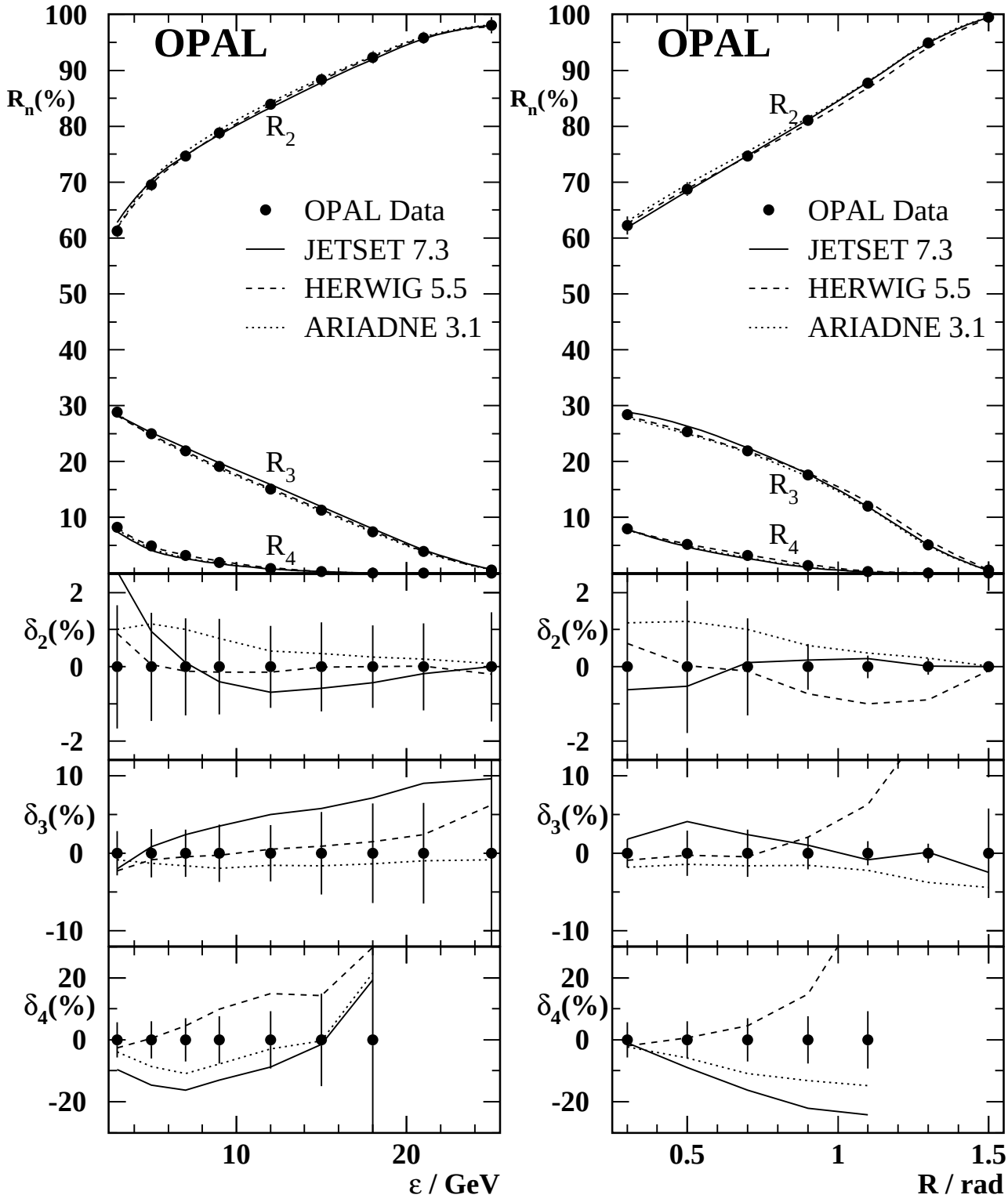

Figure 3: Measured jet rates using the cone algorithm, as a function of ε for $R = 0.7$ rad, and as a function of R for ε=7 GeV. The data have been corrected for detector effects only, and so correspond to the hadron level. The curves show the expectations of the parton shower models JETSET (solid), HERWIG (dashed) and ARIADNE (dotted). We show in the lower figures the percentage differences between the models and the data, defined as $\delta_n = 100 \cdot (R_n^{model} - R_n^{data})/R_n^{data}$, together with the experimental (statistical+systematic) uncertainties shown as points with error bars.

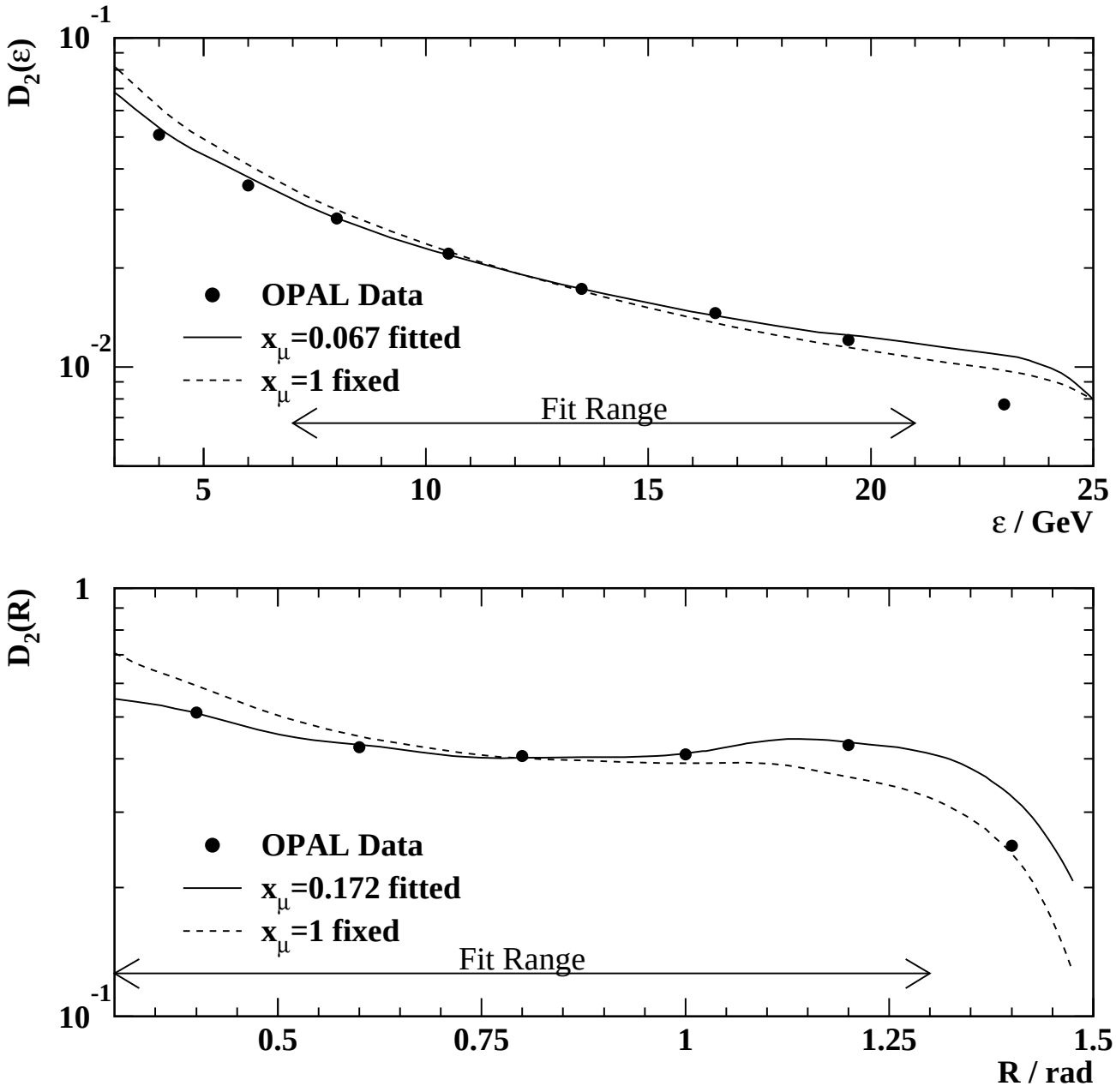

Figure 4: Measured differential two-jet rates, $D_2(\varepsilon)$ for $R = 0.7$ rad, and $D_2(R)$ for ε=7 GeV. The data have been corrected for both detector and hadronization effects, and so correspond to the parton level. The curves show the results of fitting $\mathcal{O}(\alpha_s^2)$ QCD calculations to the data: either with renormalization scale factor x_μ=1 (dashed) or with x_μ treated as a free parameter in the fit (solid). The arrows indicate the fit ranges used. The data are plotted at the bin centres; the bin edges being the same as in Table 1. The experimental errors are smaller than the symbols.

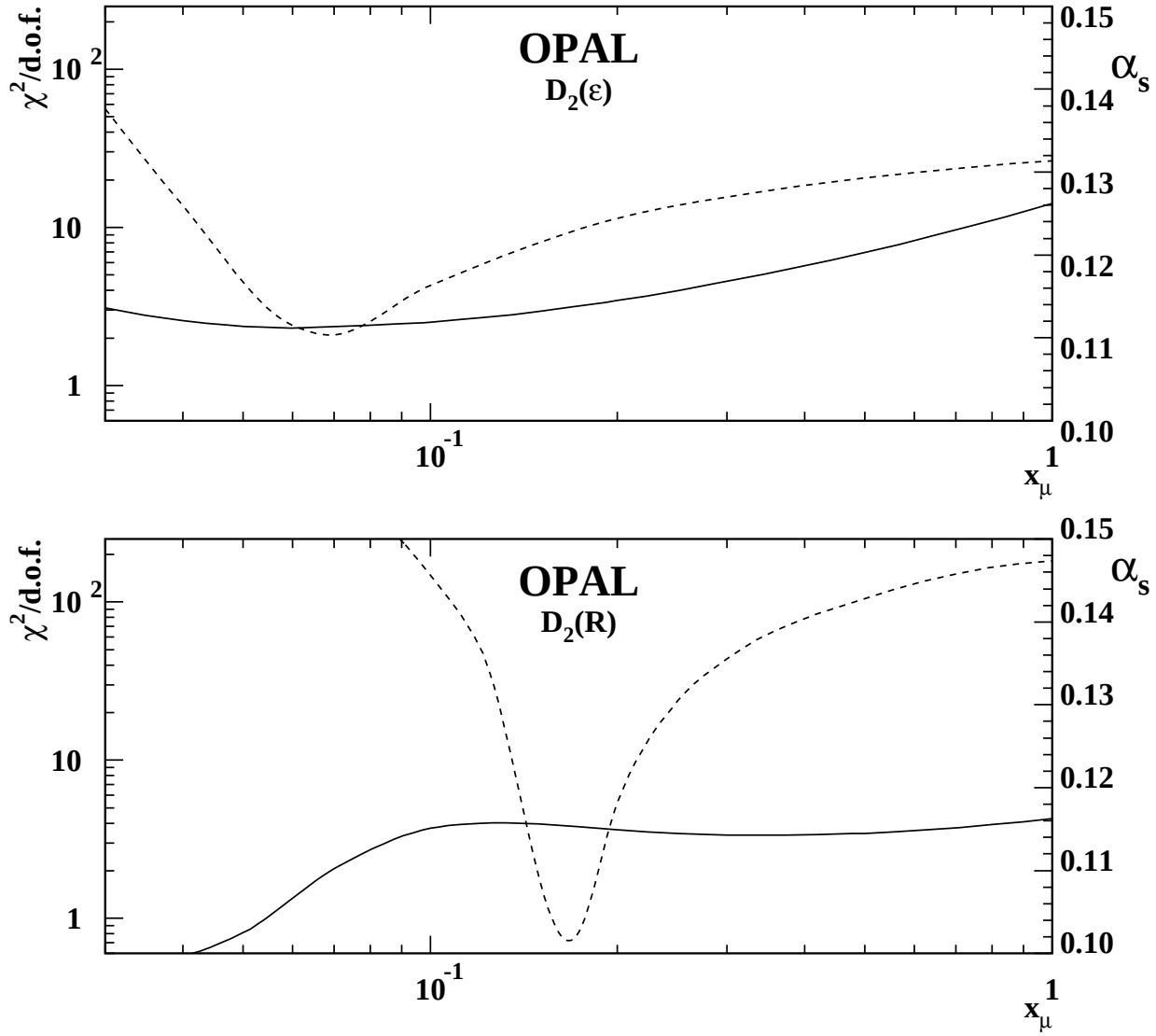

Figure 5: Dependence of the fitted value of $\alpha_s(M_{Z^0})$ (solid) and of χ^2/d.o.f. (dashed) on the renormalization scale factor x_μ for the cone jet observables $D_2(\varepsilon)$ and $D_2(R)$.

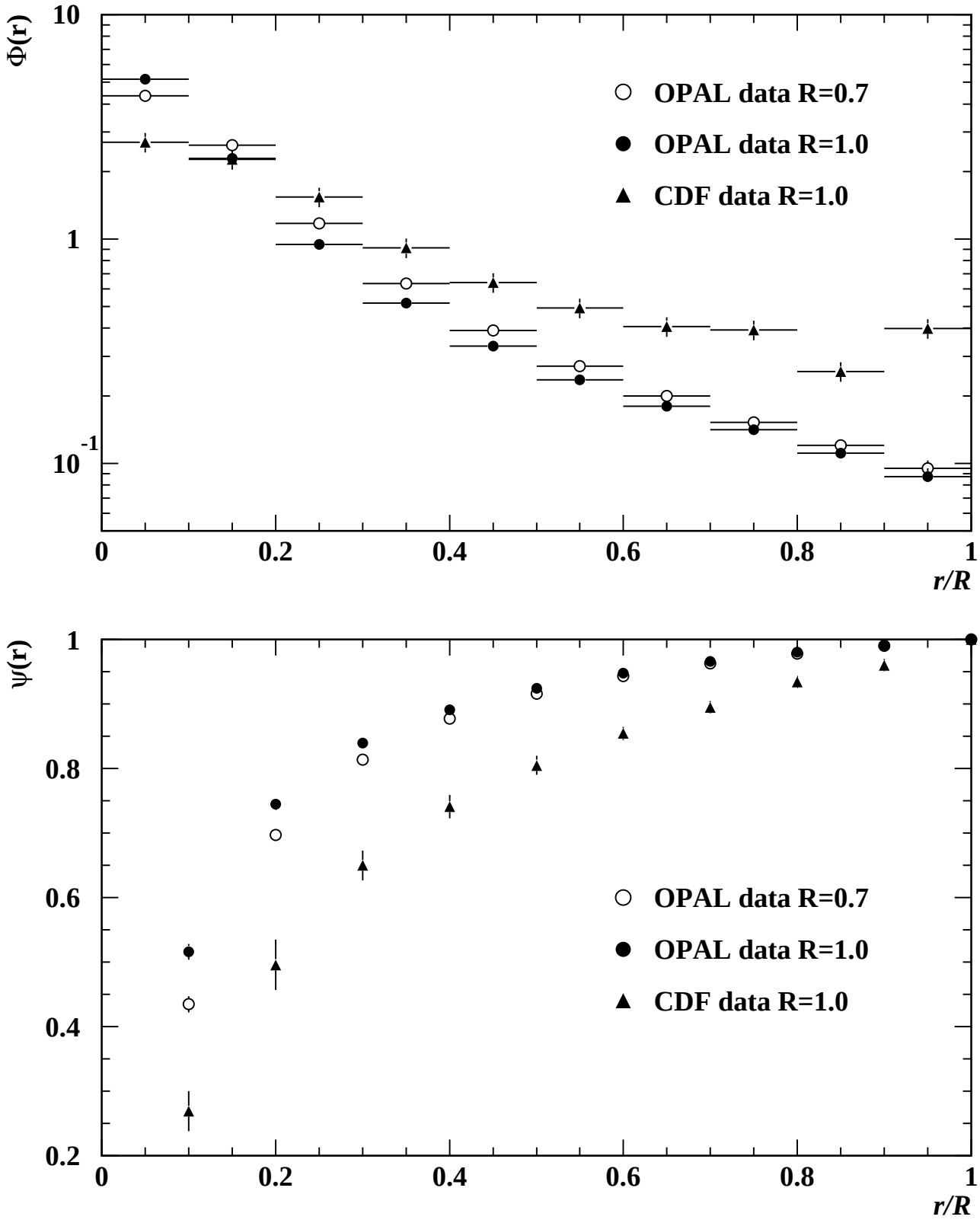

Figure 6: Energy profiles of jets defined using the cone jet finder, and having energy greater than 35 GeV. The data are shown for two values of the cone half-angle, R=0.7 rad and 1.0 rad, and use the E-χ metric. Data from CDF are shown for comparison.

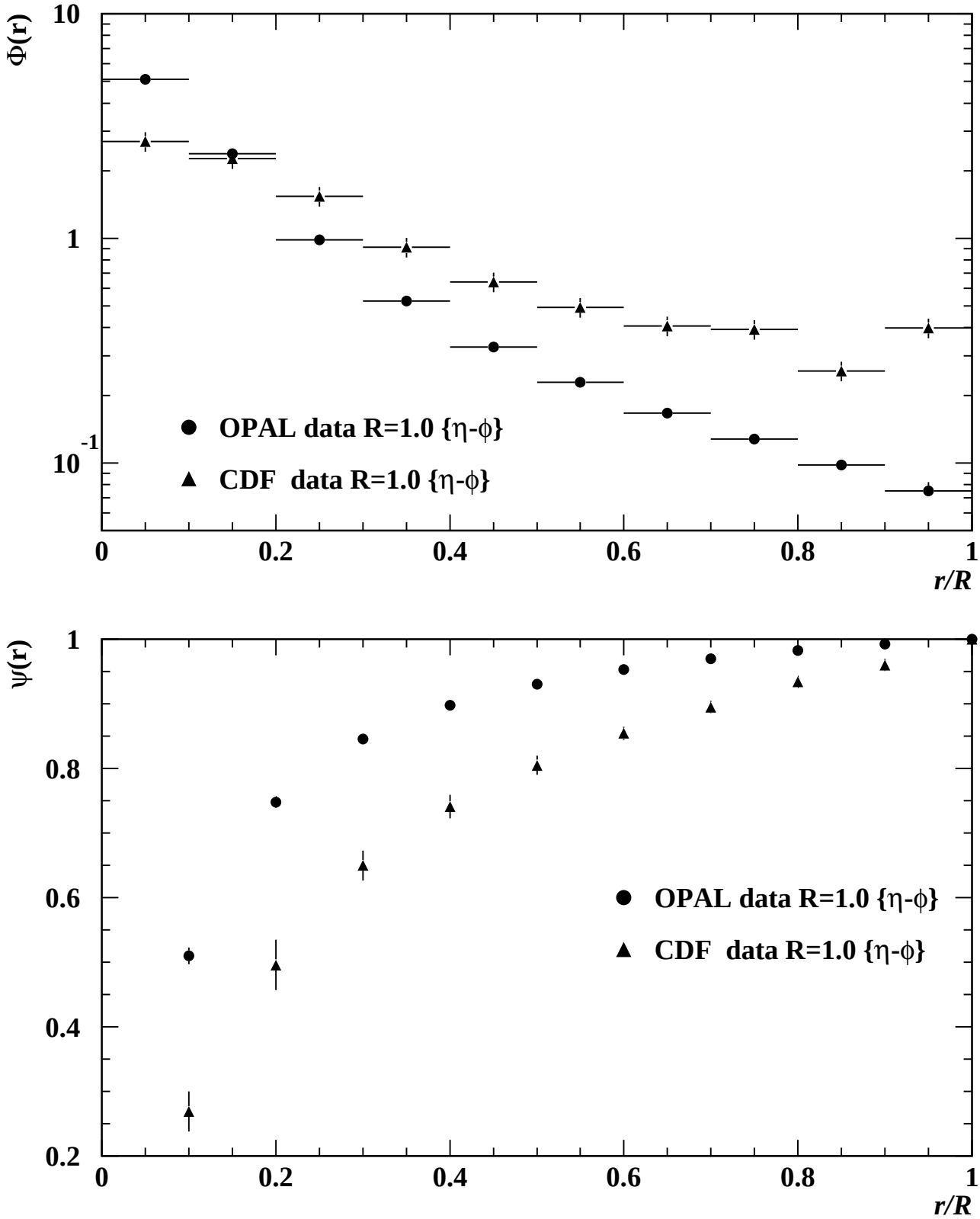

Figure 7: Energy profiles of jets defined using the cone jet finder, and having energy greater than 35 GeV. The OPAL algorithm has been modified to correspond exactly to that of CDF, i.e. defining the cone in the η-ϕ metric, cone half-angle R=1, demanding $|\eta| < 0.7$ and measuring the energy flow in terms of E_T. Data from CDF are shown for comparison.

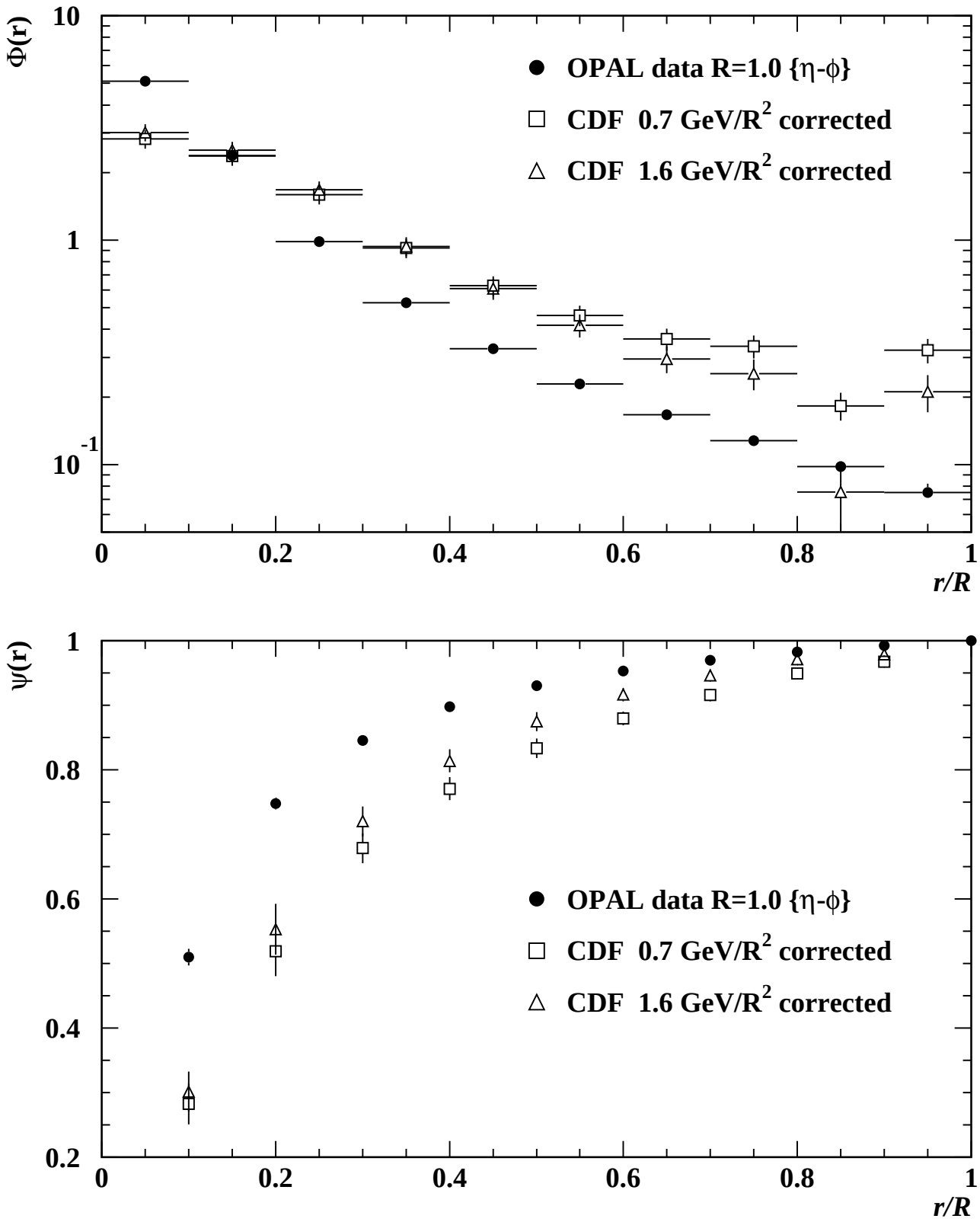

Figure 8: Energy profiles of jets defined using the cone jet finder, and having energy greater than 35 GeV. The OPAL algorithm has been modified to correspond exactly to that of CDF, i.e. defining the cone in the η-ϕ metric, cone half-angle R=1, demanding $|\eta| < 0.7$ and measuring the energy flow in terms of E_T. The CDF data have been corrected for an underlying event with an energy density of 1.6 GeV/R^2 (open triangles) and 0.7 GeV/R^2 (open squares).

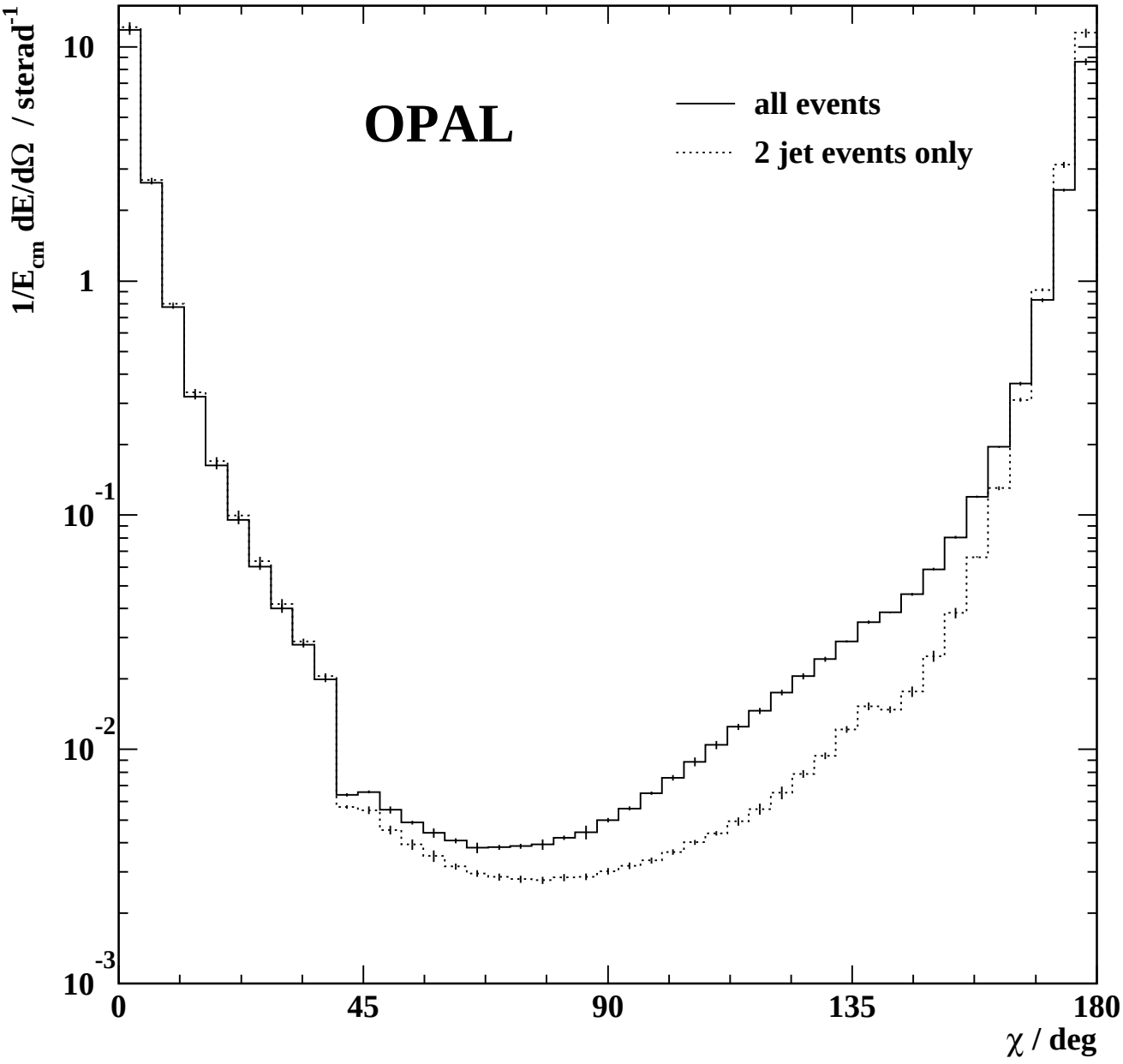

Figure 9: Energy flow per unit solid angle about the event axis for an inclusive sample of e^+e^- events (solid) and for two jets only (dotted).